The Application of Hydrofoils in high speed water craft

Third year project

Author: **Ian Duncan Godfrey** (0016011) 3rd Yr EDAT MEng

Supervisor: **Dr. S. C. Li**

Completion date: **23 / 04 / 2003**

Summary:

Watercraft can broadly be categorised by considering them as either displacement, planing or hydrofoil craft. Of these groups planing craft represent the method most commonly used for high-speed applications. The report challenges this trend by comparing the lift:drag ratio of planing and hydrofoil craft, and concluding the latter to provide a superior solution to reaching high speeds on water.

The argument is justified with a conclusive theoretical derivation of the lift over a foil and planing plate, that shows the foil to generate four times the lift and only half the drag of a planing plate of equivalent dimensions

The surfboard, a pure form of the planing craft, and a new concept in surfing, the foilboard are used as a explanatory basis for this argument. The inspiration for the argument and choice of craft comes from a piece of footage of the foilboard in action. The board flies over a meter above the waters surface supported only by a slender strut and generating next to no wake, in comparison to the large wake generated behind a traditional surfboard. The apparent absurdity with which the rider remains stable in this position whilst riding a wave prompted an investigation into the mechanics behind the situation.

As well as providing two very pure expressions of the two craft categories described, being simple, un-powered machines, the foilboard represents a new field of thinking in terms of the long standing problem of controlling foil borne craft. The product of the argument made, is the design and manufacture of a working prototype foilboard.

Contents:

Chapter 1 The history and evolution of watercraft.

From an engineering perspective, it is possible to categorise watercraft into three main groups based on the significant fluid mechanism by which they interact with the body of water. These categories are: i) Displacement hulls, ii) Planing hulls, and iii) Hydrofoil craft. The groups also represent a basic chronological evolution of watercraft, although no single concept has super-ceded the others. It is also important to point out that many craft bridge more than one of these categories, and in some case all three.

Possible further and more obscure groups of watercraft are hovercraft and ground-effect craft, although these will not be covered in the report.

1.1 Displacement hulls:

Perhaps the simplest and most widely used form of craft, the displacement hull works on the principle of buoyancy through displacement. That is, the volume of water displaced by the hull must have mass equal to the total mass of the craft in order for it to remain on the free surface of the water – 'afloat'.

Displacement hulls are designed in such a way that the hull / lower section of the craft displaces most of the water, leaving the top half of the boat, and the deck dry above the free surface. The necessity to design for this reason is one of the hindering factors of displacement hulls in terms of their achievable speed.

The typically large wetted area of a displacement hull means that they are subject to significant skin friction drag, often magnified by the fact that the low speed of the craft results in a greater likelihood of laminar flow.

To increase roll stability (rotational movement about an axis running the length of the boat), displacement hulls are often broad and bulbous in their design. This typical shape gives the hull a large frontal area around which the approaching water must flow. In order for the boat to pass through the water, it must displace water to the sides and underneath of the hull, and in doing so change its velocity (through flow direction). This change in flow velocity, and hence change in momentum (mass of the water remains constant) imparts a large retarding force on the boat.

A common solution to the low speeds of a wide-bodied displacement hull is the use of out-riggers and a very narrow hull (e.g. out-rigged canoes), a concept that later became the catamaran and trimaran, where two or three (respectively) slender hulls are placed apart and joined rigidly together above the water. The slender hulls provide a small frontal area, while the space between them and connecting structure provides god roll stability.

As a displacement hull remains on surface of a body of water, it is subject to free surface drag mechanisms such as wave drag generated in the wake of the moving boat, and surface ‘chop’ (small random-directional waves) and deep ocean waves.

1.2 Planing hulls:

Surface waves and waves generated by the craft are also a problem common to, and the most significant form of drag acting on a planing craft. Waves emanating from the rear of the craft carry energy away from it, increasing in size and effect as the speed of the craft increases.

The effect of surface chop is magnified by planing craft, as once ‘on the plane’ the craft will skim across the surface of the water, and hence is heavily subject to the quality of that surface. Planing boats can however be very fast in smooth / calm conditions, a fact utilised by most modern high-speed powerboats.

Most planing craft are adequately buoyant at rest, as a simple planing hull, but unlike pure displacement craft, the hull is shaped such that as the speed of the boat increases, water is pushed under the hull rather than to the sides, generating dynamic lift. This mechanism means that although skin friction drag has effect at the initial speed of the craft, as the boat begins plane, the wetted area is greatly reduced enabling high speeds.

A planing craft can also have negative buoyancy (will sink at rest) and still generate enough lift to keep it afloat whilst in motion. A classic example of this is the skimming stone. Although enough lift can be generated at high speed to carry large loads, to be practical, the boat must also remain afloat at rest (e.g. for loading) and hence a conflict of design between the displacement and planing hull is encountered.

The most significant form of drag, to which all pure planing craft are subject to, is spray resistance, caused by the ejection of water from the free surface by the action of the planing hull passing over the surface. This high velocity jet of water travelling in an opposing direction to the direction of travel represents a hugely inefficient los of energy from the craft. The problem of this effect is described further later in the project.

1.3 Hydrofoil craft:

A Hydrofoil works in the same way as an Aerofoil, generating lift in response to the flow of fluid over it. Even before the advent of aeroplanes, it was realised that a hydrofoils could be used to lift the hull of a boat out of the water, reducing an element of the drag imposed on the craft, and improving its ability to cope with rough surface conditions.

The increased density of the fluid in which they act, the possibility of cavitation, and the presence of a free surface boundary do present a different set of design criteria to the aerofoil, but generation of lift is the same, and is explored and derived theoretically in Chapter 4.

The surface area of the parts required to generate the same amount of lift as a planing hull is significantly less, meaning much lower skin friction drag and a greater possibility for high speeds. Once flying, foil craft are also not subject to the jet of water sprayed forward from the leading edge of a planing surface.

Although the most recent development of the three groups considered here, the hydrofoil as a method of increasing the speed threshold of watercraft has been around for over a hundred years. The first evidence for which comes from a British patent dated 1869, granted to Frenchman Emmanuel Denis Farcot [1]:

"adapting to the sides and bottom of the vessel a series or inclined planes or wedge formed pieces, which as the vessel is driven forward will have the effect of lifting it in the water and reducing the draught."

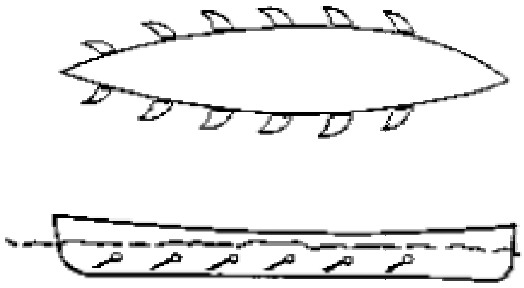

Figure 1.1 – The first documented evidence of the consideration of hydrofoils for watercraft [i1]

By 1898, Italian engineer Forlanni had designed and built a full-scale working hydrofoil, Figure 1.2. The craft shows an early realisation of the necessity for attitude control, and had an ingenious mechanism for passively controlling the flying height, later coined the 'ladder foil'. Flying height and control are covered briefly in Chapter 9.

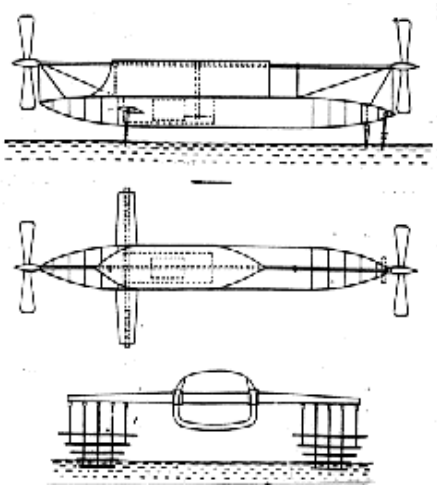

Figure 1.2 – One of the earliest examples of the successful hydrofoil craft, by engineer *Forlanni* [i2]

Although only a prototype and one of the first of its kind, the craft showed promising performance, reaching a speed of 42.5 mph, despite weighing in excess of a tonne and being driven by a primitive 60 hp engine [2]. Forlanni was the first engineer to develop some of the theory surrounding the use of hydrofoils.

The next most significant work and interest in hydrofoils came from Engineer, Professor Oscar Tietjens in the 1930's. His work covered an extensive exploration of the theory of the subject, and the development of a new self, height-controlling foil, the surface piercing foil, whereby the foils enter the water at angle (span length to free surface), and hence the amount of foil in the water varies with speed attaining constant lift.

Figure 1.3 Tietjen's *VS-7* displaying surface piercing hoop foils [i2]

The predecessor to the boat shown in Figure 1.3 reached a speed of 25 mph with only a 5 hp outboard motor, an incredible early example of the high-speed capabilities of hydrofoil craft.

Since the work of Tietjens, a large number of both successful and unsuccessful, and eccentric and simple designs have emerged, and in places taken a temporary use, or inspired short-term manufacture. The seventies saw a short period of interest with the US Navy, ferry vessels, and the emergence of sailing hydrofoil craft prompting popularity.

Figure 1.4 *USS Pegasus (PHM-1)* US Navy Patrol Combatant Hydrofoil - Missile built by Boeing Marine, launched Jun 74; first foilborne flight Feb 75; commissioned into service Jul 77. [i3]

However, despite the apparent speed potential of hydrofoils, they quickly went out of fashion after the seventies, but have remained popular with enthusiasts and ‘garden shed inventors’ ever since. More recently from the engineers and entrepreneurs amongst these enthusiasts a number of exciting new concept applications and prototypes have arisen fuelled by the development and availability of materials.

Chapter 2 The surfboard. The purest form of the application the planing surface in watercraft.

2.1 The design history of the surfboard

The history of the surfboard, much like the history of the boat can be described by the approach to design, and the development of this over a great deal of time. The ancient Polynesians have been shown to be the first surfers to use surfing as a sport and spiritual / ritual exercise. From the small amount of images available, it can clearly be seen that the first surfing craft were high volume displacement devices made from bundles of reeds, and ridden prone (lying flat on the craft).

The next significant evidence also originating from the South Pacific, comes from the voyages of Captain Cook, and his visit to Hawaii in the 1780's. This is the earliest written account of surfing and describes the craft used [3]: *'an oval piece of plank about their Size and breadth'*. The shaped wooden planks were ridden in a number of styles as depicted by Cook's artists:

Figure 2.1 Surfing Hawaiian's of 1780 – the first detailed accounts of surfing [i4]

From Cooks pictures, it can be seen that the surfboards used by the Hawaiian's and in a parallel design evolution by the Polynesians, were heavy solid hardwood planks shaped with a rounded nose and square tail, an early attempt to reduce drag and increase the energy obtained from a wave. From their size, it can be assumed that they had an amount of buoyancy, but were reliant on the ability to plane to make them functional, making them perhaps the earliest example of a planing water-craft.

The sport of surfing found its way to California in 1907, and in the quest for lighter, more manageable boards, this new breed of surfer developed the hollow board made from a wooden frame and wood veneer skins, making them very buoyant. The concept of lighter stronger boards was further developed in California in the 1960's with the advent of the shaped polyurethane foam core and thick GRP (Glass Reinforced Plastic – commonly known as 'fibre glass') skin. The boards were stronger and lighter than their predecessors, and were typically 9-11 feet (2.7-3.4) in length. This method of construction is common to todays surfboards.

2.2 The design of contemporary surfboards

The modern surfboard takes a number of forms termed, the 'Shortboard', 'Longboard' and 'Bodyboard', the most popular of which is the Shortboard. The Shortboard is typically 6 foot (1.8m) in length, and is constructed of a low-density polyurethane foam core, a thin fibre glass skin, and a hardwood strengthening stringer.

In order to make a light, responsive board, the volume of the Shortboard is kept to a minimum, reducing buoyancy. This means that whilst waiting at rest, a surfer sat on the board will only have their head and shoulders above the water level, with the rest

of the body and the board underwater. For this reason, the contemporary surfboard can be described as a planing craft, and is perhaps one of the simplest / purest examples of a planing device.

Longboards are constructed in much the same way, but are typically greater in volume due to their slower speed, and greater dependence on buoyancy. Bodyboards are made of heat-laminated layers of flexible thermoplastic foam and water proof skins. All three concepts rely on planing to function.

Chapter 3 Current innovations in hydrofoils, and the emergence of a single foil based system from the sport of surfing.

3.1 The use of hydrofoils in contemporary high-speed sailing

The advancement in displacement/planing hull design, and particularly catamarans and trimarans in sailing has slowed the commercial interest and development in hydrofoil use over the past twenty years, leaving its progress to enthusiasts. However, in recent years, the hydrofoil has made some re-appearance, particularly in water sports, conceiving some dynamic high-speed craft.

Perhaps the most successful product to date comes from *Windrider* a company specialising in one and two man racing catamarans and trimarans. The *Windrider RAVE* is one of the first commercially produced hydrofoil craft available to the general public. The boat performs well and is capable of much higher speeds than small boats of comparable size, weight and price. The success of the craft has been recognised by a new racing class currently exclusively sailed by the *RAVE*.

Figure 3.1 – The *Windrider RAVE* 'in flight' [i5]

The design, although simple, incorporates some of the most popular design features of current hydrofoil enthusiasts including *trailing wand control*, the curved black band

seen trailing from the outsides of the two outer hulls, Figure 3.1. This passive control mechanism is discussed briefly in Chapter 9. The arrangement of the three T-shaped foil assemblies is also in keeping with current thinking.

3.2 The invention of the *Airchair, Bob Wooley*.

Despite the apparent need for more than one foil to create a stable craft in motion, another recent design coming from the sport of water-skiing uses only one foil combined with a down-force wing at the rear, and mounted on a single strut.

Figure 3.2 – The Airchair foil assembly [i6]

Figure 3.3 – The Airchair in flight [i7]

Figure 3.3 shows the flying success of the Airchair, and the apparent scope for in-flight control open to the rider. The single foil and resulting low drag leave the craft very manoeuvrable, and capable of very high speeds. Figure 3.3 shows the lack of wake created by the foil.

3.3 The origin of the *Foilboard* and its application in surfing

A group of surfers led by technological pioneer Laird Hamilton took the Airchair foil assembly and attached it to a Shortboard surfboard, incorporating snowboard bindings to attach the rider's feet to the surface of the board. The device and rider were then towed by jet ski into the large deep ocean waves off the Hawaiian islands, with astounding affect. The rider was able to control the speed and direction of the foil without the tow rope, and in the critical environment of a large ocean wave

Figure 3.4 – The *Aichair* foil assembly as attached to a surfboard by *Airboard* [i8]

The Foilboard can be seen in use in the DVD - *Laird* a documentation of the surfer from which it takes its name. The Foilboard was first documented in the 1999 *Channel 4* program *Ride the Wild Surf*, covering the sport of big wave surfing in Hawaii, and it is from this material that the project takes its inspiration.

The Foilboard was commercialised by the company *Airboard* a Maui, Hawaii based group, who use the foils and developments direct from *Airchair* for their boards. The company has gained enough interest and custom to remain in existence for three years. Although successful to date, I believe the design has a lot more scope than has

currently been explored by *Airchair* and *Airboard*. The material available from the respective websites on the functioning of the foil indicates a lack of understanding of the engineering principles behind the device. Having come up with such a successful design without an apparent understanding of the device, I believe that the design still has a huge amount of design scope and application on a greater scale in water craft.

Figure 3.5 – The company offered explanation for the fluid mechanics principles behind the successful functioning of the foil [i9]

In the context of big wave surfing, the Foilboard represents a viable source of competition to the traditional Surfboard. A comparison of the fluid dynamics and mechanics of the two craft is made in this report, culminating in the design and manufacture of a prototype version of the Foilboard. Too this end, the following three chapters cover three identified areas of engineering concepts for which understanding is required prior to the design and manufacture of a prototype based on the *Airboard* Foil board.

As both the *Aichair / Airboard* foil, and the prototype foil design are referred to prior to discussion of the final design, the following diagrams describing the anatomy of both has been included in this Chapter:

Figure 3.6 – Annotated *Airchair* foil.

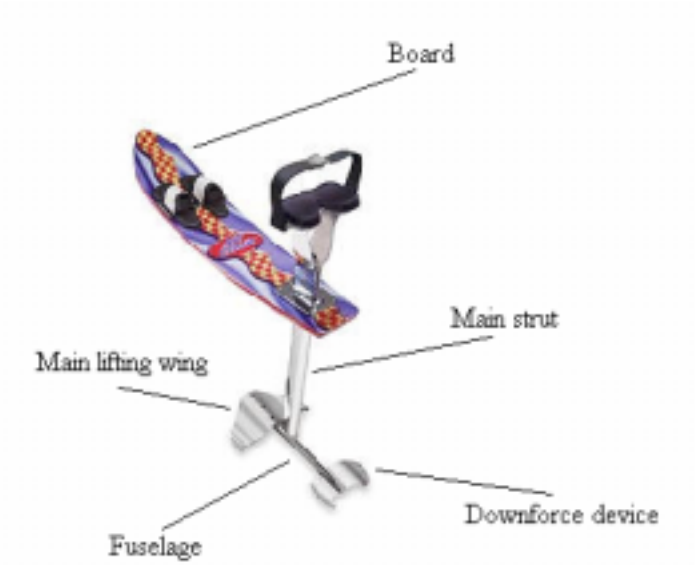

Figure 3.7 – Annotated project prototype foil

NB – exploded view to show load members.

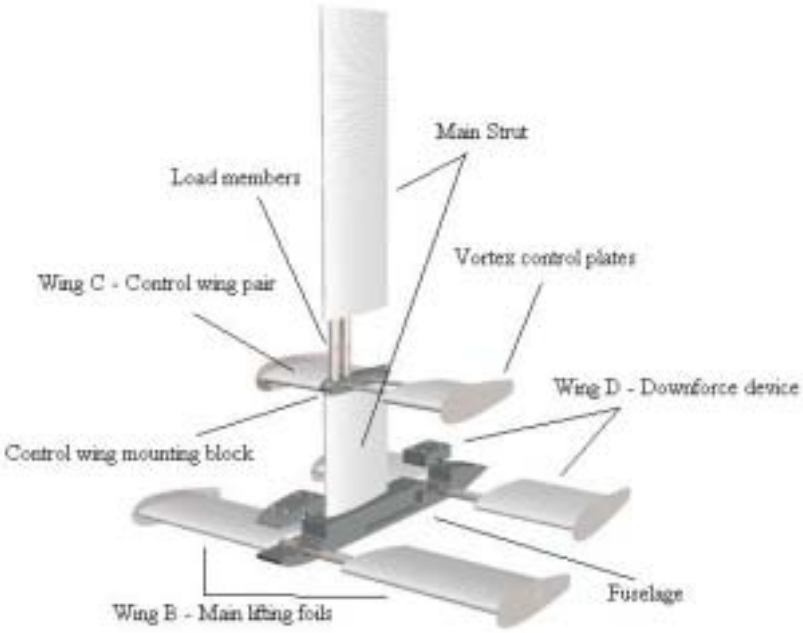

Chapter 4 The theory and arguments behind the preferential use of hydrofoils over planing devices.

4.1 Flow over a cylinder where circulation Γ = 0:

For this first step the circle (the two-dimensional projection of the cylinder) is modelled as a pair of singularity flows, a doublet, and hence the model has a net circulation of zero over the total surface of the circle. A uniform flow with velocity V_∞ (free stream velocity) is superimposed over the doublet model of the circle. Figure 4.1 describes the superimposition

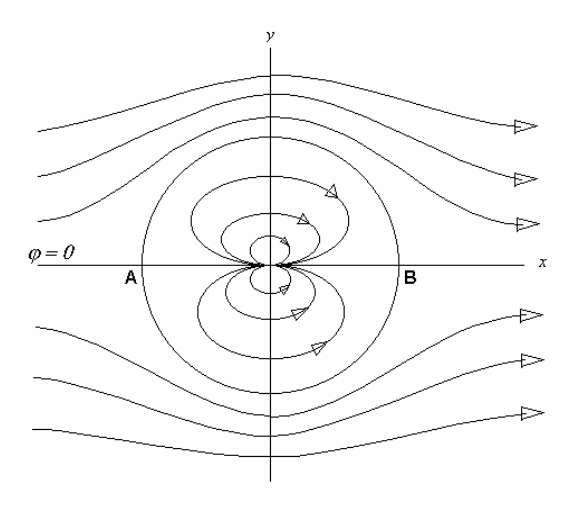

Figure 4.1 – Doublet flow, modelling the flow over a cylinder

The theoretical flow around the model can be described by the complex potential ($w(z) = \psi + \varphi$):

$$w(z) = V_\infty \left(z + \frac{a^2}{z} \right) \qquad |z| \geq a \quad \text{(i.e. circle modelled impenetrable to flow)} \quad <1>$$

where a is the radius of the circle (arbitrarily radius is r) given by the expression:

$$a = \sqrt{\left(\frac{m}{2\pi V\infty} \right)} \qquad <2>$$

m is the strength of the point sources in the doublet flow and can be expressed as a function of the free stream velocity and *a*:

$$m = 2\pi V_\infty a^2 \qquad <3>$$

On the circle, $z = ae^{i\theta}$ and from this the complex velocity can be derived in polar form:

$$v_\theta = -2V_\infty \sin\theta \qquad <4>$$

(NB the origin for the Cartesian and Polar co-ordinate systems is the same)

4.2 Flow over a circle where circulation Γ ≠ 0:

We can further modify the above model, by super-imposing a point vortex at the circle's centre, and hence introducing non-circulatory flow. A physical explanation of the superimposition of the two models is that the cylinder is now rotating:

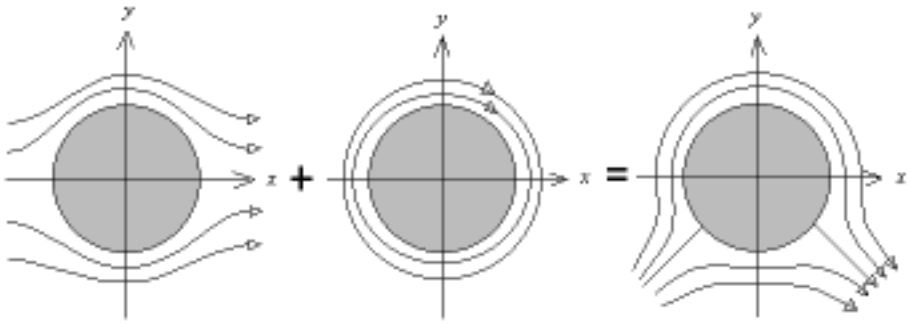

Figure 4.2.1, 4.2.2, 4.2.3 – Super imposition of non-ciculatory flow and point vortex flow

(NB – anti-clockwise rotation will be considered positive, and hence for the resultant diagram, Figure 4.2.3 above, Γ<0).

The new model generates a new complex potential that describes the flow in this superimposition:

$$w(z) = V_\infty z + V_\infty \frac{a^2}{z} + \frac{\Gamma}{2\pi i} \ln z \qquad <5>$$

The change of flow symmetry about the *x*-axis implies that the fluid passing above the circle is caused to accelerate as a result of viscous contact and transfer of momentum from the edges of the central vortex. Similarly the fluid passing under the circle is retarded as a result of contact with the vortex, and slows.

The relative variation in fluid velocity above and below the circle creates an area of lower pressure, and an area of higher pressure respectively. This effect is an example of Bernoulli's theorem (NB – gravity ignored):

$$C = p + \frac{1}{2} \rho v^2 \qquad <6>$$

This shows that the pressure at any point in the flow is solely the sum of the ambient pressure, and a component pressure proportional to the flow velocity squared, the latter of which is responsible for the generation of lift. By looking further at the components of the model and expressing them as complex potential flows, we can define this velocity.

We have already expressed the complex potential for case $\Gamma = 0$, and for the superimposed flows 2.1 and 2.2. The point vortex flow alone can be expressed by the complex potential:

$$w(z) = \frac{\Gamma \theta}{2\pi} - \frac{i\Gamma}{2\pi} \ln r \qquad <7>$$

As with equation <4>, the velocity of the fluid at the edge of the vortex ($r = a$), on the circle, can be derived and expressed in polar form:

$$v_\theta = -\frac{|\Gamma|}{2\pi a} \qquad <8>$$

The resultant expression for the velocity of two flow models superimposed is therefore the combination of equations <4> and <8>:

$$v_\theta = -2V_\infty \sin\theta + \frac{\Gamma}{2\pi a} \qquad <9>$$

This expression enables us to define the velocity of the flow at any point on the circles edge, the pressure at that point, and hence collectively the resulting lift force on the body. We begin by inputting the above velocity expression in Bernoulli's equation:

$$p = C - \frac{1}{2}\rho v^2 \qquad <10>$$

$$\therefore \qquad p = C - \frac{1}{2}\rho\left(2V_\infty \sin\theta - \frac{\Gamma}{2\pi a}\right)^2 \qquad <11>$$

$$p = C - \frac{\rho\Gamma^2}{8\pi^2 a^2} - 2\rho {V_\infty}^2 \sin^2\theta + \frac{\rho V_\infty \Gamma \sin\theta}{\pi a} \qquad <12>$$

The pressure distribution this describes can be visualized as shown here in Figure 4.3:

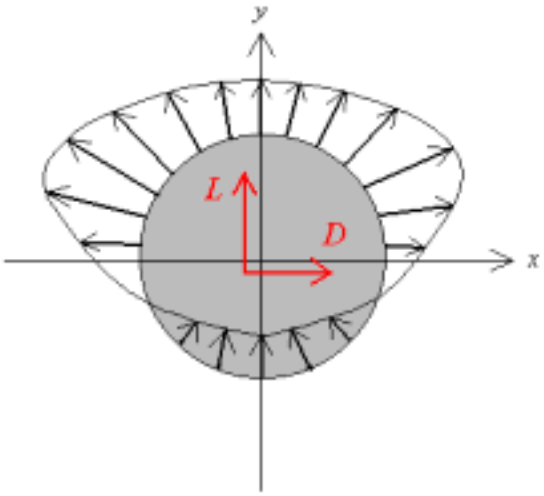

Figure 4.3 – Pressure field over the surface of the circle

The net force on the circle can be evaluated by looking at the effect of pressure on an infinitesimal arc element of its surface (assume the circle is projected into the page to generate a cylinder), then integrating to find the total force:

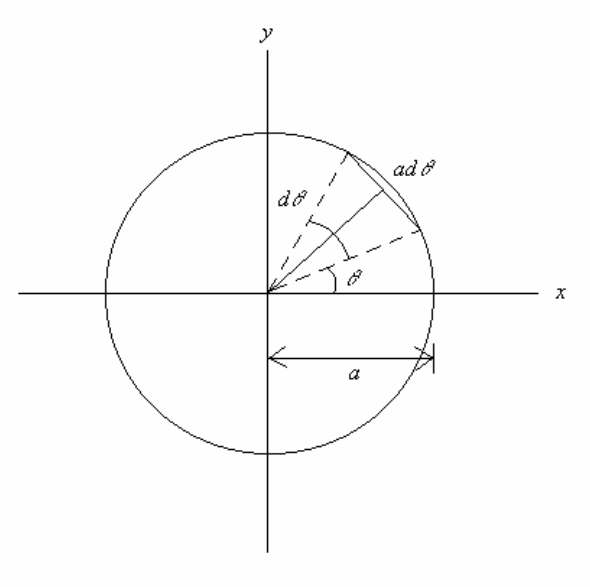

Figure 4.4 – Integration for lift force over the surface of the cylinder

The force δR on the surface of element $ad\theta$ is:

$$\delta R = pa\, d\theta\, e_r \qquad <13>$$

For each element $ad\theta$ on the surface of the cylinder, the force R can be split into an x and a y component. The x component represents the real part of complex flow model, and in physical terms, the drag generated by the circle. The y component, which for the moment is what we are interested in, represents the imaginary part, perpendicular to the free stream flow, the lift.

$$\delta R = -pa \sin\theta\, d\theta \qquad <14>$$

Integrating for the total surface:

$$R = \int_0^{2\pi} pa \sin\theta\, d\theta \qquad <15>$$

$$= \rho \int \left(2V_\infty{}^2 \sin^2 \theta - \left(\frac{V_\infty \Gamma}{\pi a} \sin \theta \right) \sin \theta \right) a \sin \theta \, d\theta \qquad <16>$$

$$= -\rho V_\infty \Gamma \qquad <17>$$

NB – $R = 0$ if $\Gamma = 0$, i.e. if the cylinder is not rotating (no circulation of flow) the cylinder generates no lift. Similarly, the amount of lift generated is related to the strength of Γ, which in turn dictates the relative positions (and appearance or not) of stagnation points A and B on the cylinder, Figure 4.1.

In complex vector form, lift is expressed:

$$= \vec{R}_L = -i\rho \vec{V}_\infty \Gamma \qquad <18>$$

4.3 Conformable transformation applied to a foil (note – a method for two-dimensional problems only)**:**

4.4

The conformable transformation method allows us to take the simple model for the lift generated over a rotating cylinder, and map the flow fields for other forms onto it using an analytical complex function *w(z)*. As the hydrofoil is geometrically most similar to the circle, we will deal with this first (and the planing surface second).

The derivation of the transformation method is most easily explained by considering major steps taken by engineers Kutta, Joukowsky, Kàrmàn and Trefftz, to generate the first mapped model of a foil, the Joukowski foil [4].

Lift on a hydrofoil: - Joukowski (Жуковский) transform and theory

Let the circle previously defined, be named *K*, and exist on plane (z), and the transform, foil *C* exist on a dissimilar plane (ζ). The mapping of the points in *K* onto C can be described by the Жуковский transform:

$$z = \frac{1}{2}\left(\zeta + \frac{b^2}{\zeta}\right) \qquad <20>$$

Where 2*b* describes the diameter of circle *K*:

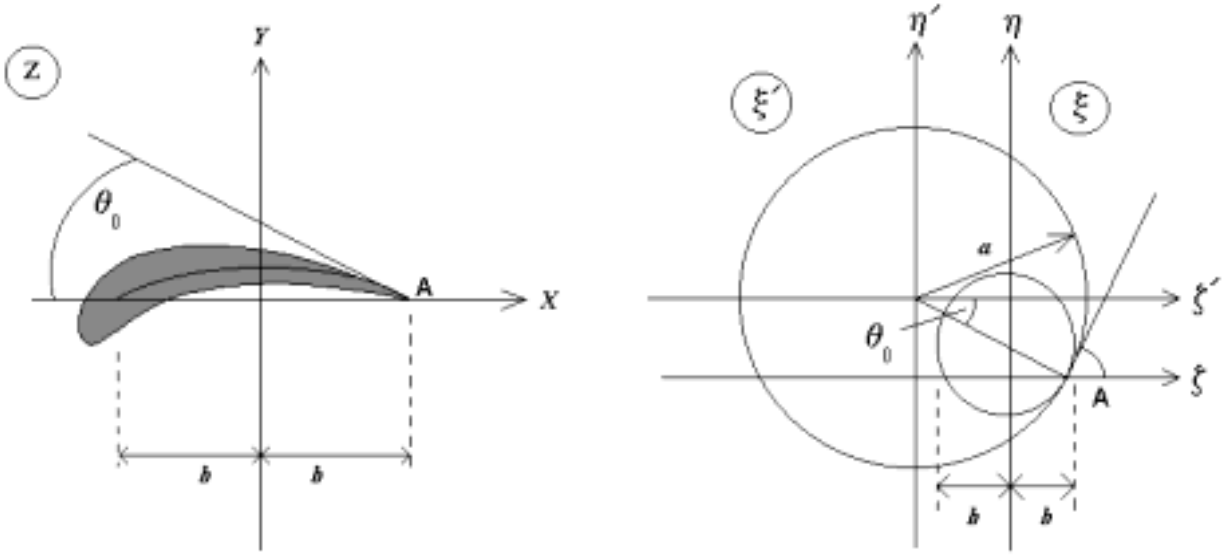

Figure 4.5 – Diagrammatic explanation of the Жуковский foil and its geometric generation. NB θ_0 represents the zero lift angle, i.e. the angle of attack for which no lift is generated by the foil.

Figure 4.5 contains one less circle than Жуковский's original transformation, a feature modified by Kutta, Kàrmàn and Trefftz to generate a foil with a finite tail angle (the internal angle between the upper and lower surfaces of the wing at the trailing edge). The larger circle, set on a new coordinate system (ζ', η') has centre ζ_o.

The transform function <20> can be used by describing an expression for ζ, and substituting this into the equation: <21>

$$z = \frac{1}{2}\left\{ b + a(\cos\theta' - \cos\beta) + ia(\sin\theta' + \sin\beta) + \frac{b^2}{b + a(\cos\theta' - \cos\beta) + ia(\sin\theta' + \sin\beta)} \right\}$$

This can be written in parametric form, from which the parametric variable θ can then be eliminated to give an expression $y = f(x)$

Flow over the Жуковский foil:

The transform function <20> satisfies the following condition at infinity for the z plane:

$$z = \infty \qquad \zeta = \infty \qquad \text{and} \qquad \left(\frac{dz}{d\zeta}\right)_{z=\infty} = \frac{1}{z} \qquad \text{<22>}$$

and hence the complex velocity dw/dz (which describes the flow over the foil) is subject to the condition:

$$\left(\frac{dw}{dz}\right)_{z=\infty} = V_\infty e^{-i\alpha} \qquad \text{<23>}$$

With the transform function, this condition can modified to show the same condition for the flow over the eccentric circle, which using the fact $\zeta' = \zeta - \zeta_0$ <24> can be expressed in terms of plane ζ:

$$\left(\frac{dw}{d\zeta}\right) = \frac{1}{2} V_\infty e^{-i\alpha} \qquad \text{<25>}$$

The complex velocity for the eccentric circle is already known (<5>) and can also be expressed in terms of plane ζ (circle centre (0,0)) due to <24>. This gives us an expression for the complex flow $dw/d\zeta$:

$$\left(\frac{dw}{d\zeta}\right)=\frac{1}{2}V_{\infty}\left[e^{-i\alpha}-\frac{a^2e^{i\alpha}}{(\zeta-\zeta_0)^2}\right]+\left(\frac{\Gamma}{2\pi i}\right)\times\left(\frac{1}{\zeta-\zeta_0}\right) \qquad <26>$$

From the Жуковский transform, we have:

$$\frac{dw}{d\zeta}=\frac{1}{2}\left(1-\frac{b^2}{\zeta^2}\right) \qquad <27>$$

Therefore, the flow over the Жуковский foil can be expressed by the complex potential:

$$\frac{dw}{dz}=\frac{\left(\frac{dw}{d\zeta}\right)}{\left(\frac{dz}{d\zeta}\right)}=\frac{\frac{1}{2}V_{\infty}\left[e^{i\alpha}-\frac{a^2e^{i\alpha}}{(\zeta-\zeta_0)}\right]+\left(\frac{\Gamma}{2\pi i}\right)\times\left(\frac{1}{\zeta-\zeta_0}\right)}{\frac{1}{2}\left(1-\frac{b^2}{\zeta^2}\right)} \qquad <28>$$

The Kutta-Жуковский condition states that:

'the circulation around an airfoil is just the right value to ensure that the flow smoothly leaves the trailing edge.'

…meaning, the complex velocity satisfies the following condition, such that the $z = b$ at the trailing edge:

$$\left(\frac{dw}{d\zeta}\right)_{z=b}\rightarrow\infty \qquad <29>$$

From this expression a finite theoretical expression for circulation Γ around the foil can be found:

$$\Gamma = -4\pi a V_\infty \sin\alpha \qquad <30>$$

which can be expressed more generally:

$$\Gamma = -4\pi R k \left|V_\infty\right| \sin(\alpha - \theta_0) \qquad <31>$$

Having found a defining value for circulation around a foil (from its complex velocity), we can express the theoretical lift of the foil, by substituting <30> into the lift equation <17>:

$$R_L = -\rho \Gamma V_\infty$$

$$= -\rho(-4\pi a V_\infty \sin\alpha) V_\infty \qquad <32>$$

(generally: $= 4\pi a V^2 \rho \sin\alpha$)

Note: - the constant terms in the expression can be collected together and used to generate an expression for the coefficient of lift C_L relative to the angle of attack α :

$$C_L = 8\pi \sin\alpha \qquad <33>$$

($R_L = V^2 \rho \frac{C_L}{2} |a|$ when angle of attack α is small) <34>

4.4 Lift on a planing surface:

The dynamic lift generated by a planing surface can also be found through an appropriate transformation of the flow field around a cylinder. The process is more complex than for the foil, and hence the theory is covered in less depth in this section.

In the same way as before, the planing plate (simply modelled in two dimensions) can be defined as a theoretical, conformable transformation of the circle, and hence a model for the complex velocity round the body can be derived.

Figure 4.6 below shows a model of the flow over the planing plate:

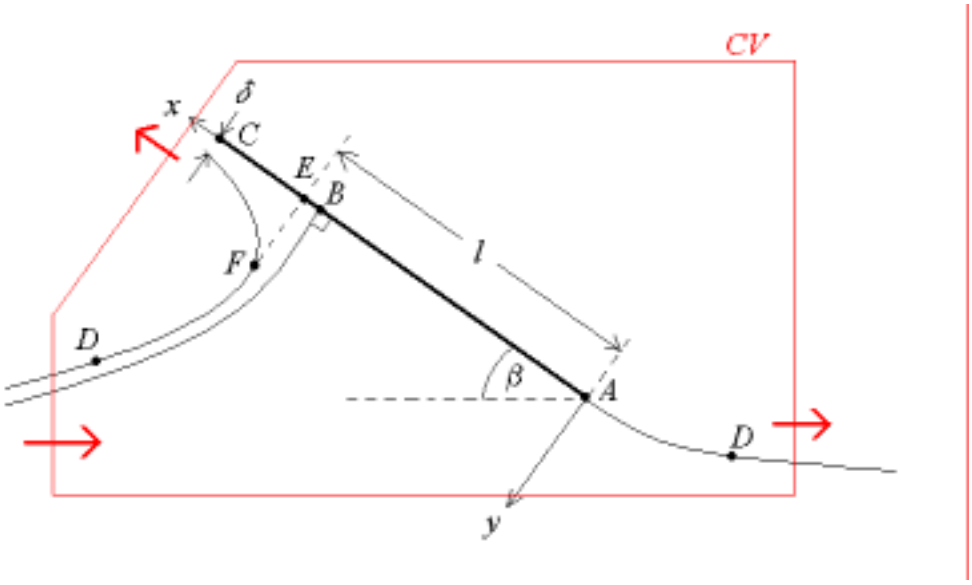

Figure 4.6 – Flow over a planing plate. Red arrows show the direction of flow in and out of the defined control volume (CV). NB the angle of attack has been exaggerated for explanation.

Tracing a loop DABCF(D) and modelling these points as a straight line, we generate an intermediate plane and associated expressions between the model of the planing plate and the flow over a fully submerged plate. By 'folding' this line about point B we join D to D (the same point) and create an effective submerged plate: (p.t.o for Figure 4.7)

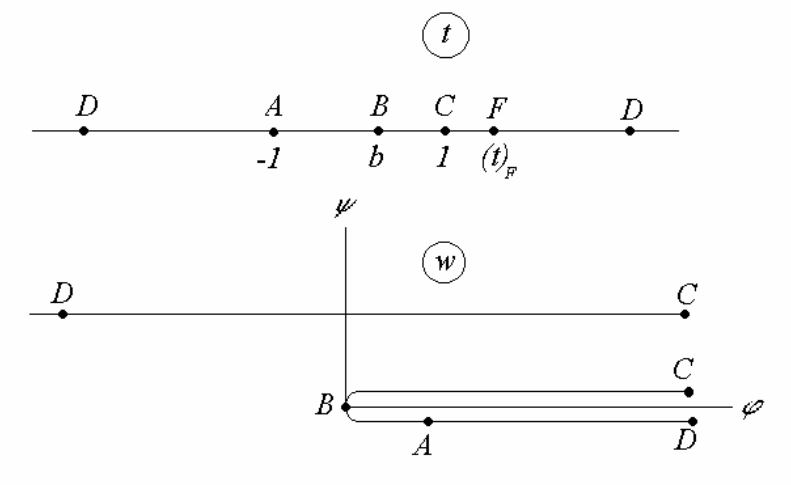

Figure 4.7 – Mapping the planing surface onto a 'fold'.

Because the un-wetted surface of the planing plate is now 'inside the fold', we remove its affect on the expression of the complex velocity, and have the ability to perform a complete integration over the plate surface to model pressure distribution, and hence calculate lift. The flow over a fully submerged plate can be found through simple transformation of the flow over a circle.

We begin the flow solution by finding a way of defining length *l*. In terms of the physical flow under the plate, length *l* is defined as the distance between the tangent to the free surface at the point where its intersection with the planing plate is perpendicular, and point A where the trailing edge of the plate. This can be expressed algebraically:

$$l = \frac{\delta}{\pi}\left[\left(\frac{1+\cos\beta}{1-\cos\beta}\right)+\pi\left(\frac{\sin\beta}{1-\cos\beta}\right)+\ln\left(\frac{2\cos\beta}{1-\cos\beta}\right)\right] \qquad <35>$$

This equation gives us the relationship between δ, β and *l*, required to generate an expression for the momentum flux over the planing surface, from which expressions for lift and drag can be derived (force equals change in momentum):

Lift: $p\cos\beta = \rho V^2 \delta \; ctg\frac{\beta}{2}\cos\beta$ <36>

Drag: $p\sin\beta = \rho V^2 \delta\left(1+\cos\beta\right)$ <37>

The momentum equation based on these expressions can be defined:

$$M = -\rho V^2\left[\frac{\delta^2\sin\beta}{\pi\left(1-\cos\beta\right)^2}\right]\times\left[L+\cos\frac{\beta}{2}+\frac{\pi}{2}\sin\beta+2\left(1-\cos\beta\right)\ln 2\right] \quad <38>$$

Both expressions <36> and <37> contain dimension δ, the thickness of jet of water expelled forwards. This is undefined and a difficult dimension to compare with those calculations made for the foil. By finding the expressions in terms of l we make a comparison with the foil lift equation.

As β tends to zero, and below around β = 10˚, equation <35> can be simplified to:

$$l = \frac{4\delta}{\pi\beta^2} \quad <39>$$

Substituting this into <36> and <37>:

Lift: $L = \frac{\rho v^2 l}{2}\pi\beta$ <40>

Drag: $D = \frac{\rho v^2 l}{2}\pi\beta$ <41>

Similarly, a good approximation for momentum can be given:

$$M \approx -\rho\frac{v^2}{2}l\pi\beta\frac{3l}{4} \quad <42>$$

The fraction that appears in the last term of this expression gives us the pitching moment position, situated ¾ of *l* from the trailing edge. This is equivalent, and the same as the position of the centre of effort on a foil.

4.5 Theoretical comparison of the lift generated by foil and a planing surface:

Having generated an expression for the lift over a planing surface in terms *l*, we are now in a position to directly compare the expressions. The length term *a* given in equation <32> can be expressed: $a = ½\ l$. This is due to the way in which model for the planing plate is generated, and is best understood by considering the original definition of *a*, Figure 9 (5). Given this condition, we can write the foil lift equation:

$$R_L = 4\pi \frac{l}{2} v^2 \rho \sin\alpha$$

$$= 2\pi\, l\, v^2 \rho \sin\alpha \qquad <43>$$

For small α: $R_L = 2\pi\ l\rho\alpha$

Attack angle terms α and β are the same in value for every angle:

For the foil: Lift: $R_L = 2v^2 l\pi\alpha$

For the planning plate: Lift: $L = \frac{1}{2} v^2 l\pi\beta$ <44>

Hence the lift generated by a foil is theoretically four times greater than that found for a planing plate of the same chord, and hence the same area. **Q.E.D**

Comparison of drag:

Although it is possible to generate a theoretical proof for the drag over the planing plate and hydrofoil using Жуковский's methods, the content of its derivation falls outside of the scope of this project, being long and complex [7].

The mechanisms of drag discussed in Chapter 1 can be shown to give a planing plate a drag twice that of a hydrofoil of equivalent plan area, despite the surface area in contact with the water being only half. This phenomenon is partly as a result of forward thrust generated by the pressure field over the surface of a wing, and partly due to the large splash resistance created at the leading edge of a planing craft. This feature can be seen in Figure 4.6, represented as a jet of water ejected in an opposing direction to the direction of travel. Newton's third law dictates that this change in momentum of the water imparts a force opposing the forward motion of the planing craft and contributing significantly to drag.

Chapter 5 The mechanics of riding a conventional surfboard and the contemporary rival, the foilboard.

5.1 The mechanics of riding the foilboard.

From the information available on the current foils, the ideas and input of Dr. Li and myself, an initial design concept was generated. After deliberation over mechanics of the current device, the model expressed in Figure 5.1 was suggested in order to form a backbone for the design of a prototype.

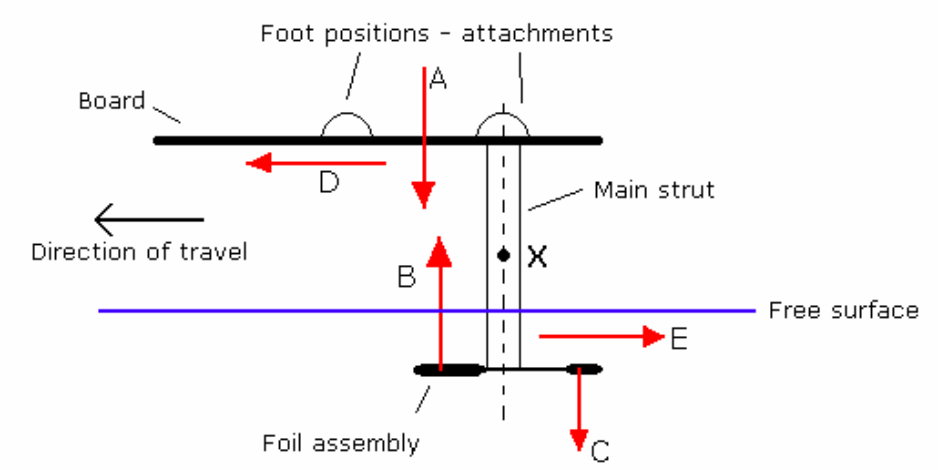

Figure 5.1 Basic anatomy of the current Foilboard design, showing significant identified forces A-F

Forces A to F represent the significant forces identified for this model. Force A is the combined weight of the board and rider, assumed to act through the riders centre of mass. Forces B and C represent the lift (and down-force) generated by the front and rear foils respectively (see Figure 5.2 / 3) and forces D and E represent the applied thrust and resistance forces respectively.

A stable surfing / riding position is achieved by the rider adjusting their centre of mass such that the moments of A, B and C about point X are in equilibrium. This idea is explored in greater depth in Chapter 6, for its actual surfing application. Although

initially an unexpected observation, Figure 5.4 shows clearly the downward angle of attack on the Rear foil, implying a negative lift, or downforce.

The companies concerned were naturally unkeen to divulge the dimensions and design details of their products, and without sufficient resources to buy the parts for study, very approximate measurements have been taken from close study of stills taken from the DVD – *Laird* featuring footage of discussion on and riding of the Foilboard.

Figure 5.1 shows an example of the foilboard, but is given as an example of the design, and was not used for dimensions. Figures 5.2 shows an estimate of the dimensions of the foil design.

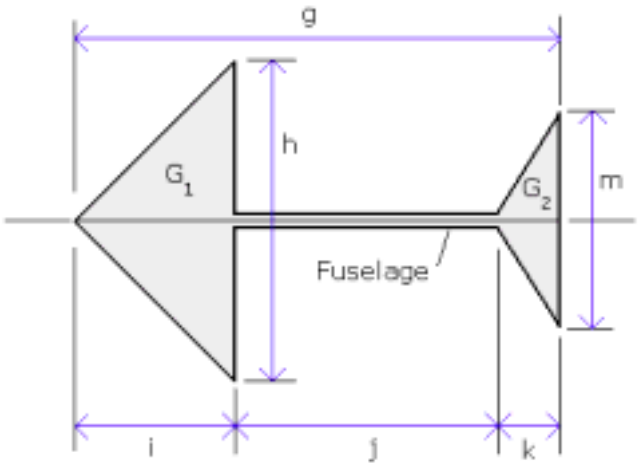

Figure 5.2 **Left: An example of a Foilboard, showing the two triangular foils at the base of the main strut**

Figure 5.3 **Right: A plan view of the foil assembly, showing the front and rear foils.**

The measurements made are tabulated in below:

Dimension			Foil Area		
g	=	550mm	G_1	=	$0.036m^2$
h	=	360mm	G_2	=	$0.015m^2$
i	=	200mm			

j = 250mm

k = 100mm

m = 300mm

The measurements taken were used to make the first estimates at wing size and aspect ratio for use in the CFD package discussed in Chapter 7. A database of the sizes considered can also be found in Table 7.1 – Appendix B.

5.2 Initial design concept

This section contains figures taken from work with the CFD. These values are only approximations, based on more sophisticated versions of the common lift and drag formulae. The validity of these figures will be discussed in greater detail later.

In order to simplify the design, it was decided that rectangular plan wings, and a constant section design should be used in order to simplify their manufacture (see Chapter 8). Keeping all the foil components the same section and chord meant that a faster more accurate form of manufacture could be generated in the time and with the budget available. The rough dimensions for the Foilboard were used to make a first guess at the chord length for the sections of the prototype. It is possible, but unlikely that the delta shaped foils found on the current design provide an element of increased control at high angles of attack, e.g. during take-off. However, the effects of stall are less significant with hydrofoils than with Airfoils, and hence the use of rectangular plan foils should be successful.

Another possible explanation for the tapering wings on the current design is to minimise the loss of lift due to wing tip vortices. Further evidence of attempts to minimise tip vortices can be seen in curved down wing tips of the current design (Figure 5.4). The

greater the lifting area near the tip of a wing, the greater the likelihood of lift energy lost in the generation of useless tip vortices. For this reason, it was deemed necessary to build end plates into wings of the prototype, in an attempt to interrupt flow from the lower to upper surfaces of the wing and hence minimise the loss of lift as a result of tip vortices. These features can also be seen in the Airchair foil.

Figure 5.4 A modified version of the Airchair foil, showing the foil assembly and detail of the turned down wingtips used for reducing wingtip votices. [i10]

By making an estimate at the chord length of the section to be used, and making the assumption that for the areas of section generating lift (subject to force), that force acts at the quarter-chord position, its possible to generate a force model for the prototype. This force model can then be used to pick the required wingspan for the lifting surfaces (see CFD work in Chapter 7), and make choices over the structural elements of the design and likely modes and areas of failure.

From the outset, it was decided that an attempt would be made to incorporate a simple form of height control, based on the many constant lift ideas that have appeared in hydrofoil design over the past hundred years. This was manifested in a simple pair of control wings, Wing C, mounted on the main strut (see drawing in Appendix A). As an arbitrary design figure, it was decided that the lift force required would be shared between these wings and the main lifting (Front wings) in a 30:70% ratio respectively. Their position on the main strut was similarly chosen as being 30% of the total length from the foil assembly to the board, with a minimum distance of 200mm to avoid conflict of flow fields around the main foils.

The force diagram, Figure 5.1, takes into account the presence of a towrope, and the force that this imparts on the rider and hence the board. The board must be able to function under tow, in order to get the rider up to flying speed, and without the presence of a tow boat, whilst surfing. The lack of suitable surf in this country, and for reasons of safety the device has been designed solely for use under tow, although it is assumed that a surfer competent in the sport would be able to ride the board on a wave.

5.3 Assigning values and performing calculations

The calculations below for the final design of the prototype have been carried out a number of times before and during the design process. Initially the calculations were carried out on the current Foilboard as taken from the DVD stills, to gain an understanding of the figures involved, and to build a basic specification for the materials required for the manufacture of a prototype.

This first set of calculations produced estimated figures for the lift generated by the Front (Wing B - area G_1) and Rear (Wing D - area G_2) foils shown in Figure 5.2. The combined weight of the rider and board was estimated at 900 N, in hindsight, possibly a slightly conservative guess given the build of the surfers using the board.

Lift on Wing B = 1300N (to 2 sig. Fig.)

Lift on Wing D = - 420N (")

These figures imply a torque at the joint between the fuselage and the main strut, and similarly at the connection between the board and main strut of approximately:

$$\left(\left(120\times10^{-3}\right)\times1300\right)+\left(\left(270\times10^{-3}\right)\times420\right)=270\,Nm$$

Details of the assumptions made and the original hand calculations are given in Calculations 5.1 – Appendix C.

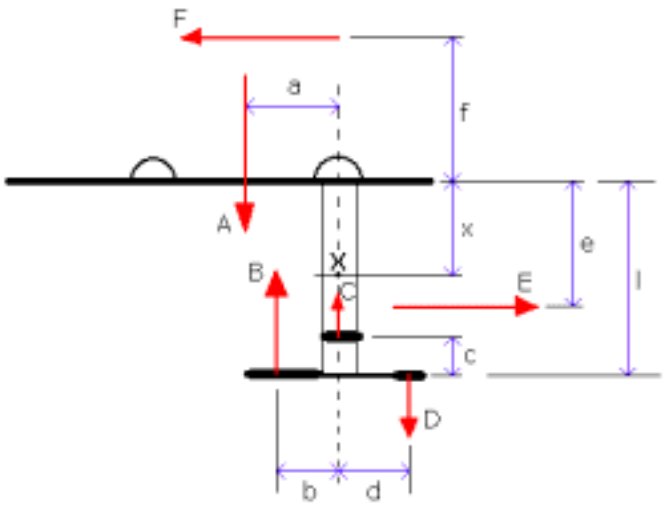

Forces considered:

A -Weight of the rider and equipment.

B - Main wing (Wing B) lift force.

C - Control wing (Wing C) lift force.

D - Downforce wing (Wing D) lift force.

E - Cumulative drag on foils and strut.

F - Thrust force from tow rope through rider

Figure 5.5 Force model for considering the mechanics of the prototype concept. Again, force vectors are indicated with red arrows.

Assuming a quarter chord position for the centre of pressure (CP – the point through which *B*,*C* and *D* act) on each foil, and taking the standard section to have a chord length of 180mm (the value chosen for the final design – Table 7.1), the dimensions a-f specified in Figure 5.5 can be quantified. NB – a small study [8] of the quarter chord design principle is given in Appendix D

***a*- 0.4m** (Assumed to act, on average, mid-way between the span of the feet)

***b*- 0.135m** (= 0.75×180) (Trailing edge of wing sits at centre of strut chord)

***c*- 0.2m** (NB – CP of Wing C is assumed to act through point **X**)

***d*- 0.25m**

e*- 0.63m

f* - 1.5m*

* The value for the total drag force *E*, can be approximated using CFD software, and is given in the list below. Taking drag to be proportional to frontal area, the centre of area

for the proposed design was found, and taken as an approximate position to model the point of action of *E*. The distance to this position is denoted *e*.

** The distance between the board and the height of the towrope as held by the rider. The value given is a rough estimate, and is likely to vary significantly during towing.

Similarly, some values for A-F can be estimated prior to calculation;

A **- 700 N** (Assuming rider mass m_r = 70 Kg, and g = 9.8 ms^2)

E **- 46 N** (CFD approximation)

Point X, has been taken as a what appears to be the most logical point around which to resolve moments, although its position may need to be reconsidered after testing

Calculations:

Total Lift: $L_T = B + C$ <5.1>

As specified above: $B = 0.7L_T$ <5.2>

$C = 0.3L_T$ <5.3>

Resolving forces vertically: $A + D = B + C$ <5.4>

$700 = B - D + C$

Substituting in <5.1>: $B + C = L_T \quad \therefore \quad 700 = L_T - D$

<5.5>

Substituting in <5.2>: $L_T = 0.7B \quad \therefore \quad 700 = \frac{B}{0.7} - D$

$0.7(700 + D) = B$

$490 + 0.7D = B$ <5.6>

Resolving forces horizontally: $F = E$ <5.7>

$\therefore$ ***F* = 46 N**

Moments about point X: $Aa + Ff = Bb + Cc + Dd$ <5.8>

(NB – *C* is designed to act through point X)

Substituting known values: $(700 \times 0.4) + (46 \times 1.5) = 0.135B + 0.25D + (46 \times 0.63)$

$320.02 = 0.135B + 0.25D$ <5.9>

Substituting in <5.6>: $320.02 = 0.135 \times (490 + 0.7D) + 0.25D$

***D* = 737 N** (to 3 sig. fig)

B can be now found by substituting *D* into <5.9>:

$320.02 = 0.135B + (0.25 \times 737)$

***B* = 1010 N** (to 3 sig. fig.)

C can be found by substituting *B* and *D* into <5.4>:

$700 + 737 - 1010 = C$

***C* = 427 N** (to 3 sig. fig.)

From these values it was possible to explore wing dimensions in order to find appropriate spans (having set the chord dimension) for wings B,C and D. The values are also essential for choosing the correct load bearing members carrying the wings, and for those running the length of the strut. These aspects are covered in Chapters 7 and 8 respectively.

Correction for manufacturing error:

On completing the first prototype wing, it was realised that the moulds had been mistakenly undersized. A function of Pro Desktop 2001 entitled ‘offset-chain’ was used to offset the original designed section of the wing to account for a 1mm skin of GRP

(two layers of 0.5mm fabric). The effect of the function is however greatly exaggerated when applied to a sharp bend, as can be seen in the sharp trailing edge, resulting in an un-noticed shortening in length greater than 2mm (as planned – 1mm at the leading edge, and 1mm at the trailing edge. The problem was further magnified when the new smaller profile was then used to generate the moulds discussed in Chapter 8. For the manufacture of the moulds, the profile was offset by a further 0.5mm to generate 'rib' profiles accumulating further error.

The result of this error is that all wings produced from the moulds have a chord 8-10mm shorter than proposed. Having inadvertently adjusted dimensions *b* and *d*, the calculations were re-run to check the affect on load values found for the design. The re-worked calculations were also used to account for a more comfortable narrower rider stance, and a greater rider weight, after concluding that the mass of the equipment had been initially underestimated:

New estimate for A' = 800 N (based on a 70Kg rider and 10Kg of equipment)

With new rider stance a' = 0.3 m

With new 17mm chord b' = 0.12 m

d was left unchanged, and the wings position on the fuselage adjusted accordingly instead.

The new values found: ***B* = 1030 N**

***C* = 440 N**

***D* = 680 N**

Chapter 6 The hydrodynamics of surfing a wave – the real estate of the surfer

6.1 The dynamic real estate of the surfer – the face of the wave.

Surfers serious about the sport are very particular about the waves they ride, meaning that certain locations ('Waves') around the world are more preferable than others, having suitable topography (local ocean floor), weather and swell consistency. Waves in a 'good' spot can be found to be surprisingly regular and predictable, meaning that with a little time spent studying the wave; the formidable task of the surfer can be made more manageable.

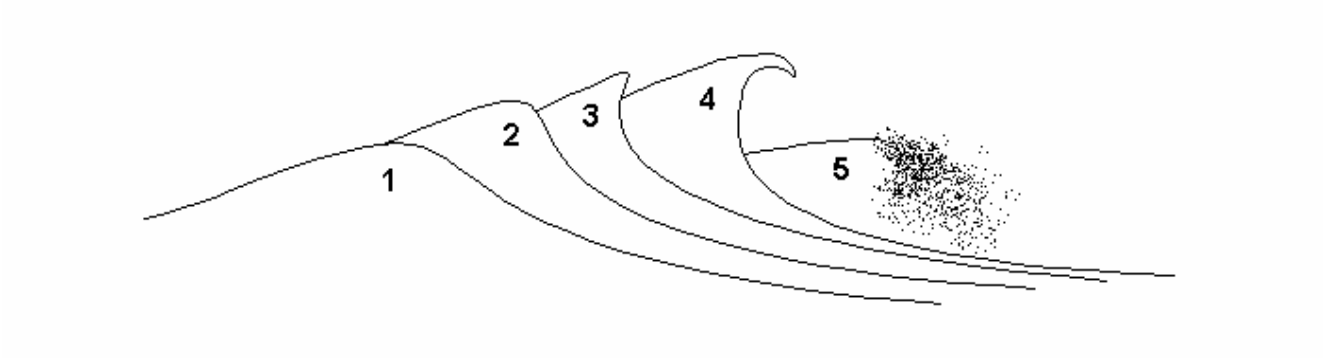

Figure 5.1 A wave 'breaking' as it travels into shallow water.

Figures 5.1 and 5.2 show the typical profiles of a desirable surfing wave as it breaks, changing from shape 1 to shape 5 as it gets close to shore (Figure 5.2). As waves typically approach a beach in lines that are not parallel to the shore, part of the wave will reach shallower water first. This factor means that the various progressive stages (1-5) of 'breaking' appear to travel along the length of the wave, as seen in Figure 5.2.

(p.t.o for Figure 5.2)

Figure 5.2 A breaking wave, as seen from the shore. The breaking section of the wave is travelling from left to right. [i11]

A surfer will typically attempt to occupy the leading face of the wave at stages 3 and 4. In order to carry this out successfully, they must therefore travel across the wave as seen from the shore, moving with the progressive breaking of the wave. The accomplished surfer will try to remain as close to the turbulent 'white' water as possible, without getting caught in it, positioning themselves in the steepest part of the wave, tucked under the pitching lip of the wave.

Figure 5.3 An accomplished surfer riding the critical section of the wave.

Anatomy of the wave:

Ocean waves are trochoidal in profile, meaning that the crests are sharper than the troughs. However, for the purpose of understanding the transmission of a wave through a volume of water, we will consider the wave as sinusoidal, shown in Figure 6.4:

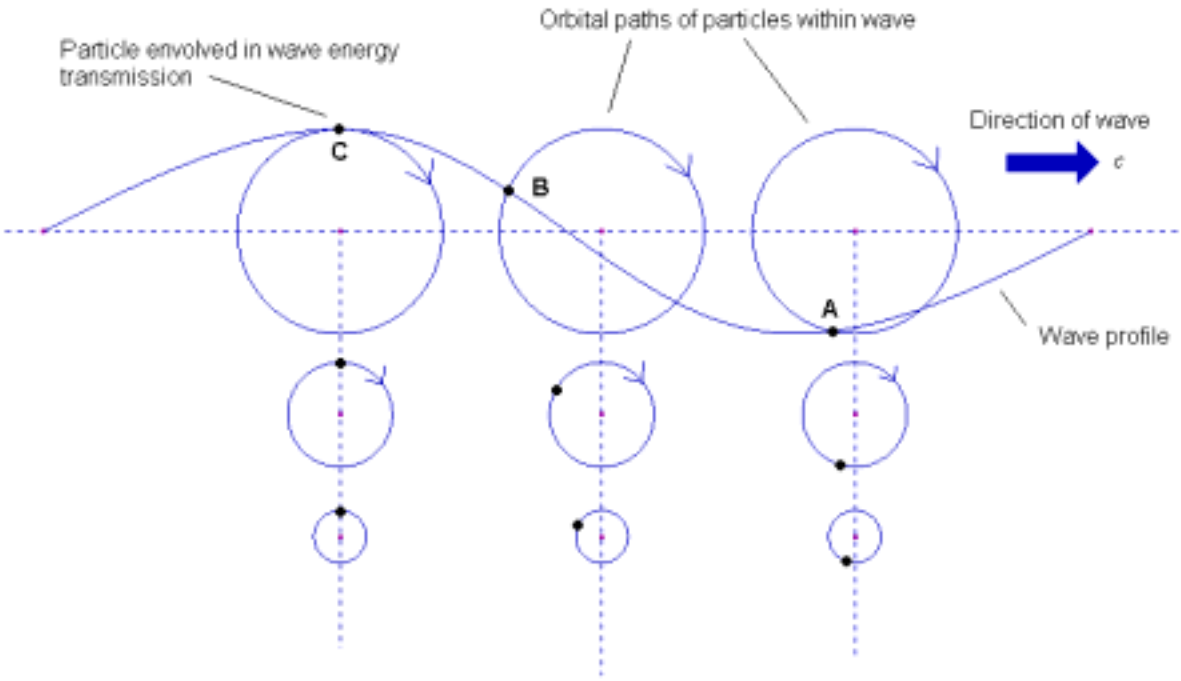

Figure 6.4 - The anatomy of a deep, ocean wave.

The motion of the wave can be modelled by considering the motion of any particle in the volume of water through which the wave is travelling. The three points **A, B** and **C** shown, are three arbitrary positions in the sinusoidal cycle of the wave. As time progresses, point **A** moves clockwise around the orbit to the equivalent position of point **B**, and then that of point **C**, travelling up the face of the wave. The particle has no net displacement over time, indicating that from a relative perspective, it is the wave that moves, and not the water. In order for a surfer to remain on the leading face of the wave, the aim of surfing, their net speed must be such that they travel down the

face of the wave at the same speed that a particle translates from point **A** to point **C** (in the opposing direction).

As can be seen from Figure 6.4, the orbital motion of particles in the wave is repeated as we go deeper below the free surface of the wave, although with diminishing effect, represented by the reduction in orbit diameter. It is this anatomy of the wave that causes it to finally collapse into turbulent flow (‘break’) as it approaches a coastline, or area of shallow water.

Until the wave breaks, the translation of particles from the trough of a wave to its peak is a constant pattern, meaning that from the surfers perspective, the slope on which they are travelling is constantly being renewed. The surfer therefore, effectively has an infinite slope down which to ride, assuming the wave never breaks.

6.2 The mechanics of riding a conventional surfboard

The model below is a greatly simplified example of the reality of the typical surfing position shown in Figure 6.3, where the surfer traverses the face of the wave, rarely riding straight down the face. The model however, can be used to make a valid comparison with the foilboard, especially as the foilboard will typically be used on much larger offshore ocean waves, where the localised effect of travelling across the wave on a surfboard are greatly reduced [9].

If we model the surfer as remaining in one relative position on the profile of the wave as it travels, we can approximate this infinite slope to a flat ramp of gradient equal to the tangent of the waves free surface at that point (free surface angle γ). By modelling

the surfer as though they are at a constant relative position on the wave, we therefore assume that an equilibrium of forces acts on the board and surfer:

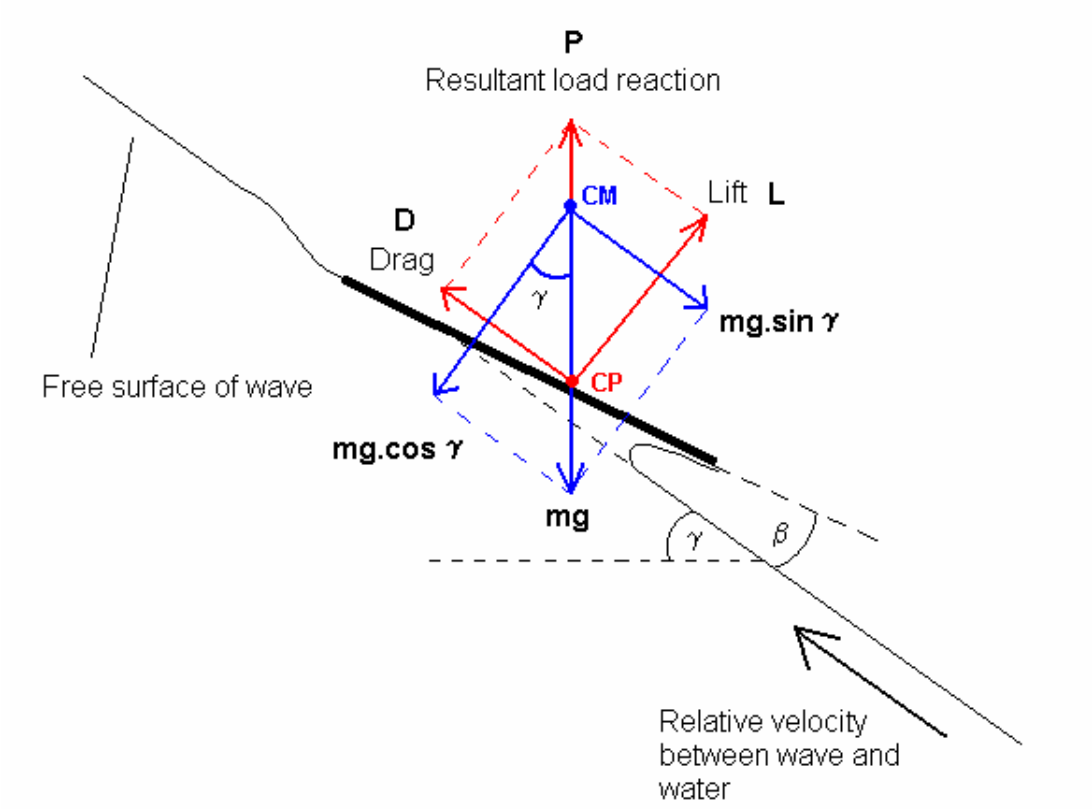

Figure 6.5 - A simple model for the mechanics of riding a conventional surfboard

The reality of this state of force equilibrium is expressed by modelling the surfer as having reached terminal velocity, meaning they cease to accelerate down the face of the wave. At this point, the drag generated is exactly equal to the component of the riders weight acting parallel to the slope of the wave ($mg.sin\gamma$).

The weight (mg) of the surfer can be said to act vertically downwards from a point defining their centre of mass (CM). The board itself is assumed to be of negligible mass and volume, and hence neutral buoyancy. In this state of equilibrium, the resultant force (P) from the dynamic lift (L) and drag forces (D) generated by the

planing surface acts parallel to and in the opposite direction to the surfers weight, and through point CP.

Point CP is the centre of pressure on the planing surface (moment about this point = 0), and occurs at approximately a quarter of l from the leading edge of the planing area (l is the length of the planing area in effect at any point in time – see Chapter 4).

By adjusting their position on the board, the surfer can control its angle of attack (β), or 'trim' and hence wetted / planing area, and in doing so the lift, drag and direction and magnitude of resultant force P. Here in lies the art and skill of surfing, controlling the board with the attitude of the rider's body, and in doing so maintaining a state of equilibrium that enables the surfer to stay on the face of the wave.

It is important to note that it is both the drag and lift on the surfboard that enable the surfer to maintain equilibrium, where drag is commonly perceived as a hindering factor. However, by reducing the drag, we can achieve the desired state of equilibrium at a higher (terminal) speed.

With drag reduced by as much as a factor of four for the same lift, the foilboard enables the surfer to travel at a much higher speed. As the size of a wave (its amplitude and wavelength) increases, so does its speed, to the extent that a surfer wishing to ride a wave in the range 8 – 10m will need to travel at a speed of 40 - 50knots (20.5 – 25.7ms^{-1}) to remain on the wave's face.

We will now consider the rather more complex force equilibrium model of the surfer riding the foilboard. The situation is described in Figure 6.6.

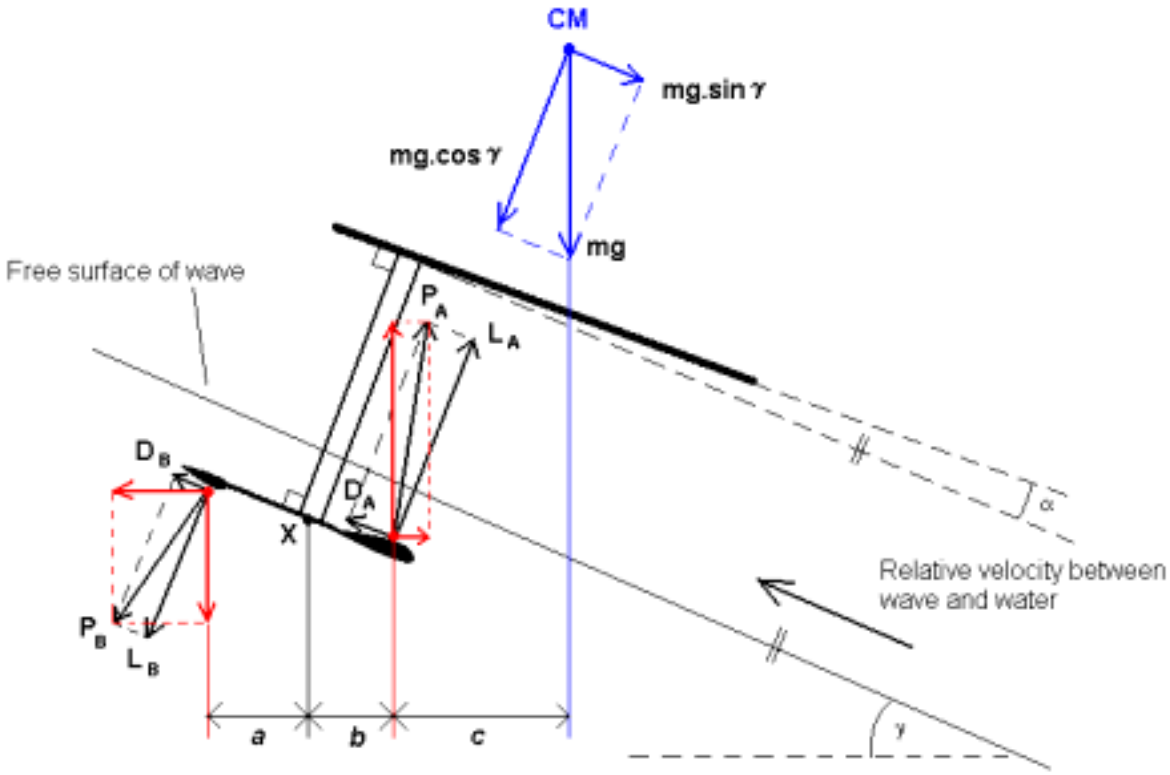

Figure 6.6 - A simple model for the mechanics of riding the Foilboard.

As in case of the planing surfboard, it is the reaction to the rider's weight that determines whether they fly at a constant height above the free surface, and the drag of the parts underwater that determines the terminal speed at which the surfer ceases to accelerate, and a state of force equilibrium is achieved.

The foilboard surfer must achieve a balance whereby the moment generated about point X by the combined affect of the two foils (A and B) is equal to the opposing moment generated by the rider's weight. In order to do this, we separate the resultant forces, P_B and P_A into horizontal and vertical components (represented by the red arrows). The surfer now has to trim the board, adjusting the angle of attack α such

that the following expression holds. P_{BV} and P_{AV} are the vertical components of P_A and P_B respectively:

$$(P_{BV} \times a) + (P_{AV} \times b) = mg \times (b + c)$$

The steeper the wave, the further back the surfer must move their centre of mass, bringing weight over the back foot, and reducing the moment about point X.

Chapter 7 Theoretical design of the lifting surfaces and understanding of flow over the foilboard assembly.

7.1 Computational Fluid Dynamics, and the use of Hanley Innovations, *Visual Foil Lite 4.0*.

The expense and lack of facilities for valid water tunnel / channel scale model testing of the work in the project has meant a certain dependence on CFD (Computational Fluid Dynamics) for results and validation of design work. Although a wind tunnel and appropriate formulae can be used to simulate bodies submersed in fluids other than air, it is very difficult to model the presence of a free surface, a significant factor in the working of the foilboard. The CFD package used for the project is also unable to model a free surface, but represents a more justifiable use of time than testing in the wind tunnel.

The full-scale prototype once complete, will act as a base for experimental work, either mounted on a rig attached to a boat, or with a surfer / rider under tow. To this end, the device has been designed with fully adjustable main foils, which can be removed and replaced with alternative components. The main strut, board, and fuselage are also separable, making replacement and adjustment possible.

Further work will involve extensive testing of the prototype, including the installation of strain gauges, flow speed and pressure measurement that can be linked to a data logger. The project plan was to provide simple test results from the prototype for the

conclusion of this report, and although complete, it was not possible to test the finished device.

Although a useful tool, CFD however sophisticated, can only provide a theoretical model for flow patterns, which in the case of turbulent flow, are highly complex and chaotic. Results from CFD work can be very inaccurate and misleading, and hence should be considered with caution when using them for design purposes. For this report, only simple CFD work has been used, and will require testing of the prototype to validate it.

To enable some basic CFD work, *Hanley Innovation's Visual Foil 4.0 Lite*, was purchased for the project enabling accurate analysis and selection of wing sections, and providing NACA coded profiles that can be manipulated and exported for use in CAD. The package includes a section called *Airfoil Doctor*, a sub-program where design criteria for a given wing can be input. Figures 7.1, 7.2 and 7.3 show the input fields and output of *Airfoil Doctor*.

Figure 7.1 Input fields in *Airfoil Doctor*

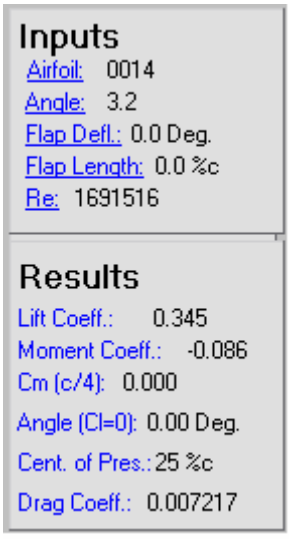

Figure 7.2 The NACA code and AOA are specified at the start of a session. Results for C_L are specified in the main program.

Figure 7.3 **Output values from *Airfoil Doctor*. These values were used to generate spreadsheets: Table 7.1 & 7.2.**

7.2 The choice of foil and performance predictions based on specification requirement.

From the outset of the project, it was decided that to keep the initial prototype simple, fitting its design and manufacture into the time and budget available, a symmetric section wing should be used, for all parts of the assembly. NACA 4 digit sections are the most commonly used source of simple section wings, and if only the last two digits are varied, produce symmetric profiles:

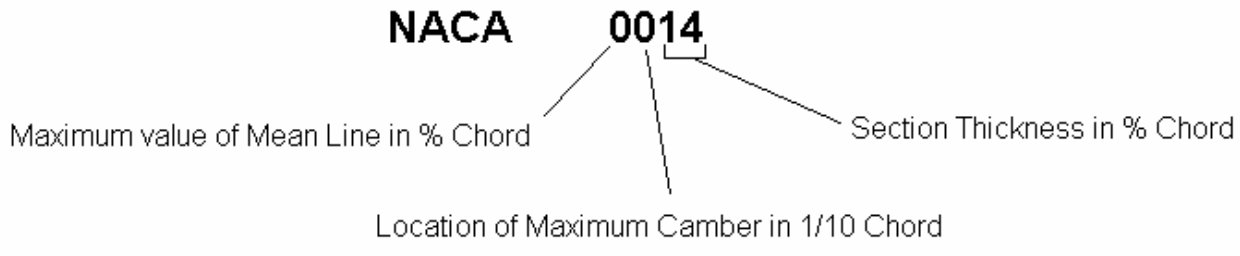

The program then uses the NACA code to generate a co-ordinate map of the section profile:

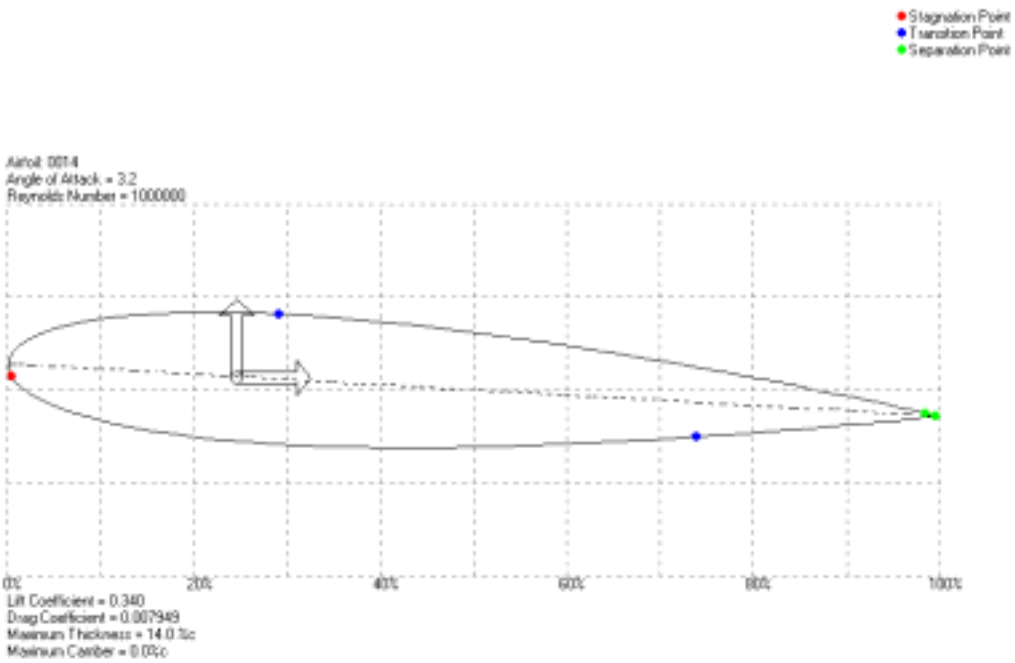

Figure 7.4 – Co-ordinate map of the foil section NACA 0014, at 3 degrees AOA.

Lift response to changes in angle of attack

The use of a thicker foil than that seen on the Airchair foil was decided following discussion over the affect of angle of attack (AOA) on symmetric foils. Simple CFD work can be used to show that the thicker a foil is, the lesser the effect of varying AOA has on lift. For the rider controlling the AOA of the foil the sensitivity to change in lift is important.

DVD footage of the Airchair foil in use, shows that the foil regularly generates too much lift, almost instantly causing it to rise to the free surface, where cavitation of the foil causes all lift to be lost at once. The loss of lift causes the board to land on the

free surface, increasing drag and slowing the surfer until enough speed is generated to bring the board back into flying mode.

Although this process does not appear to be detrimental to the rider, it does emphasise the knife-edge region of control open to the rider. By using a thicker foil, the device is hindered by more drag and slightly less lift (at lower AOA), but should provide a more 'forgiving' ride for the surfer, allowing more freedom of movement and a better sense of control over the board.

These factors were explored and validated using *Visual Foil* and are shown in Table 7.1 (Appendix B) and Graph 7.1 (below). Three NACA sections are shown (arbitrarily the dimensions of Wing B were used), of varying thickness / volume. In Graph 7.1, both thinner foils, 0005 (series 1) and 0010 (series 2) can be seen to generate more lift than 0015 (series 3) until both eventually stall, first 0005, then 0010, causing detrimental loss of lift and inefficient flying for any greater AOA.

Graph 7.1 - to show the effect of foil thickness on lift at varying AOA

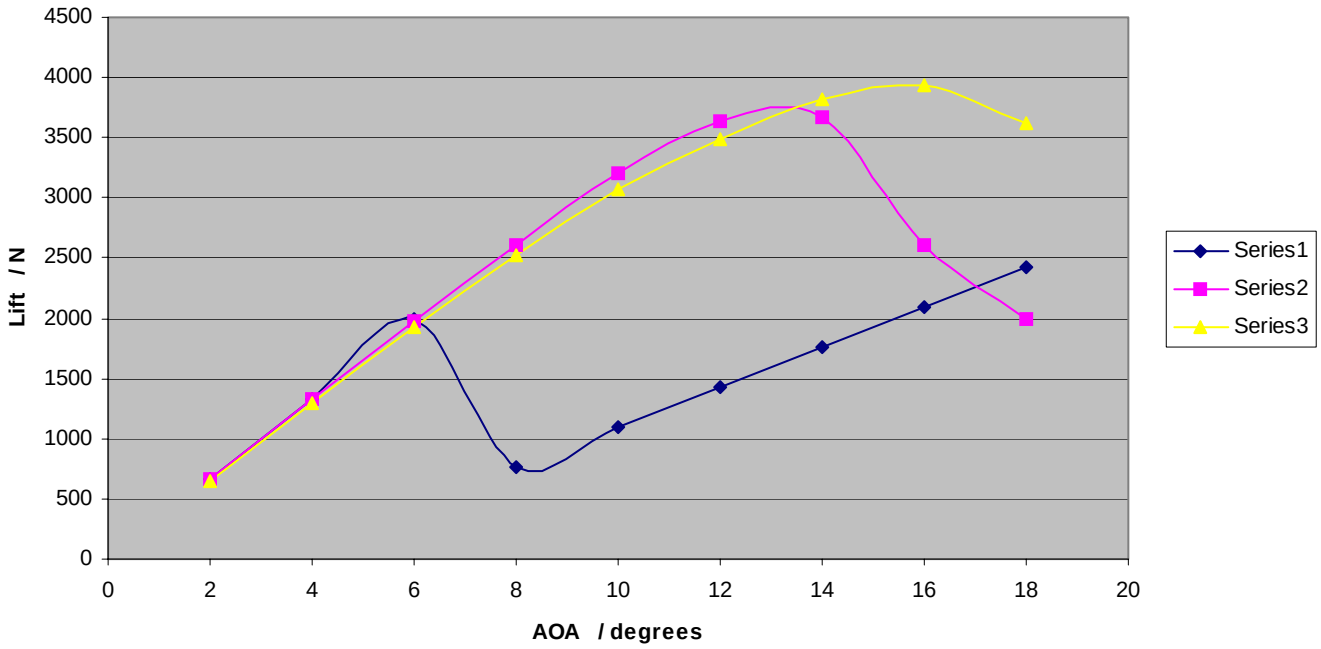

Stall is further factor supporting the use of thicker foils, as 0015 can only begin to be seen to stall at around 16°, and is a much slower process, giving the rider more time to adjust the attitude of the board accordingly.

The CFD results for drag of varying thickness' of foil are unclear (Graph 7.2) but indicate that at the desired operating AOA (≈ 3° - see later in text), the profile drag is much the same for all three. Perhaps more significantly, the lift:drag ratio (Graph 7.3), indicating the working efficiency of the foils in the expected operating range is lower for the thicker foils. This opposite boundary condition sets a design decision – making a compromise between the control of foil, and the efficiency, and hence its ultimate speed.

Graph 7.2 - to show the effect of foil thickness on drag at varying AOA

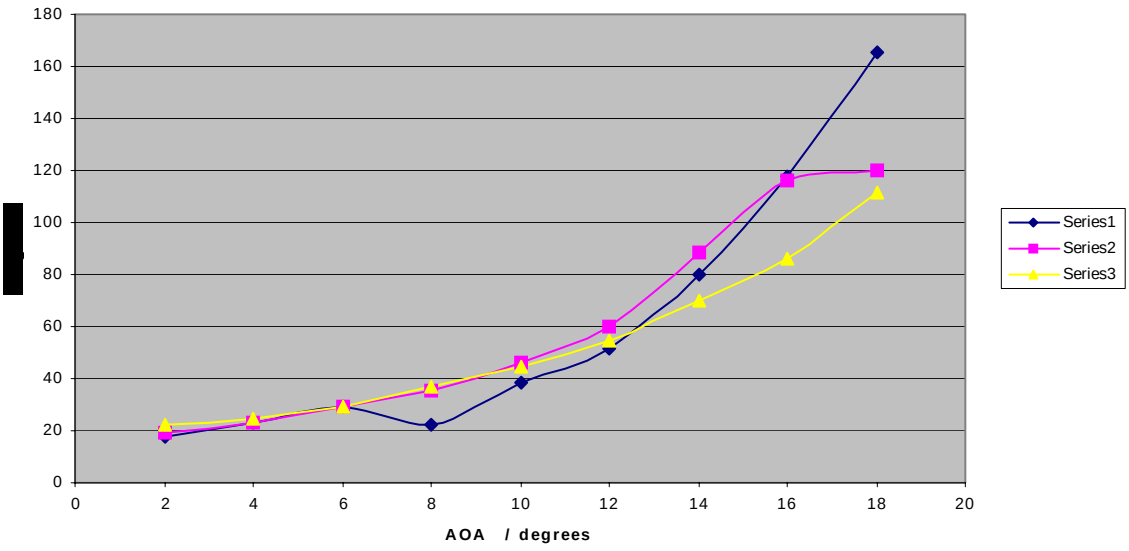

Graph 7.3 - to show the effect of foil thickness on lift:drag ratio for varying AOA

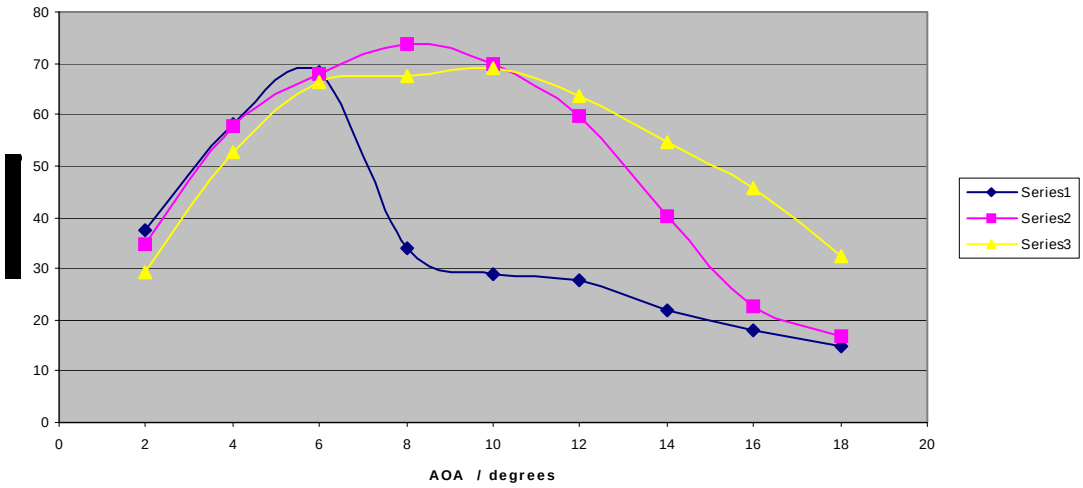

The thickness of the foils is also governed by the need to contain a structural member(s) within the section to make the wings capable of withstanding the large loads anticipated. After generating Paper models from the DXF exported profiles from *Visual Foil*, it was decided that NACA 0014 would provide a suitable compromise, and be capable of containing suitable load bearing members.

Choosing the optimum AOA

The desired operating AOA range for the foil can be identified by considering a C_D vs. C_L plot for the chosen NACA code. The $C_L.C_D$ plots for the three foil sections discussed above, and the chosen section 0014 can be seen in Graphs 7.4 and 7.5 respectively. Graph 7.5 shows a red line running tangential to the curve, and through the origin. As the gradient of the red line reduces (its position becomes closer to the *x*-axis), we approach the 'ideal' foil such that $C_L \rightarrow \infty$ and $C_D \rightarrow 0$, implying a foil with infinite lift and zero drag (opposite to the *y*-axis).

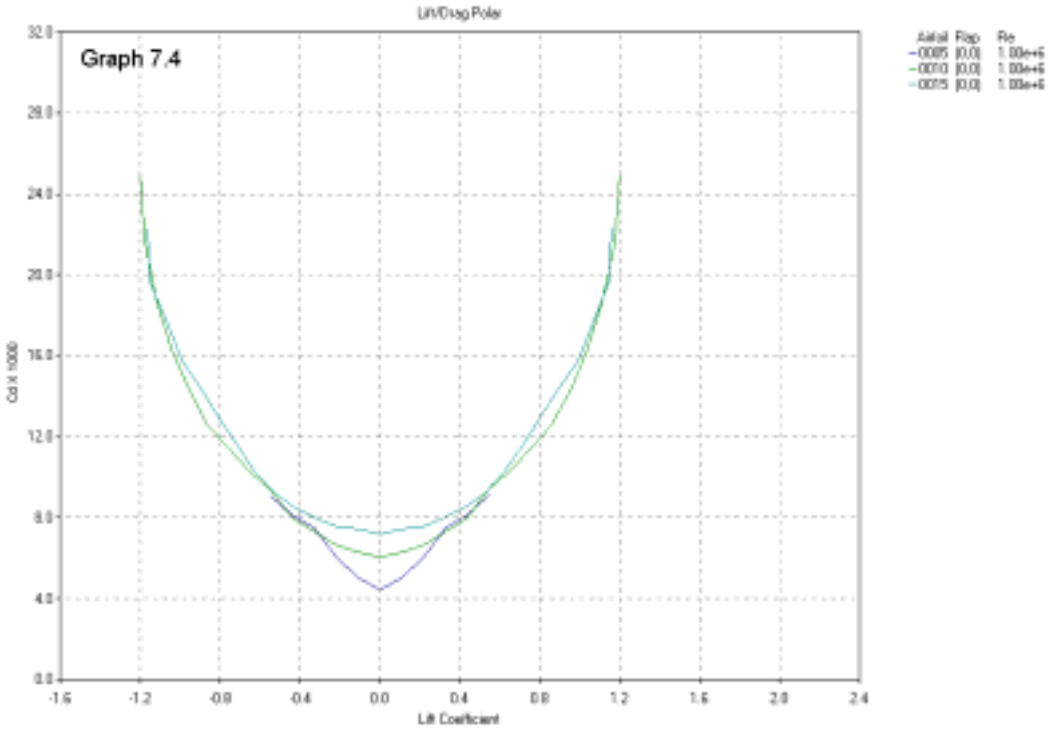

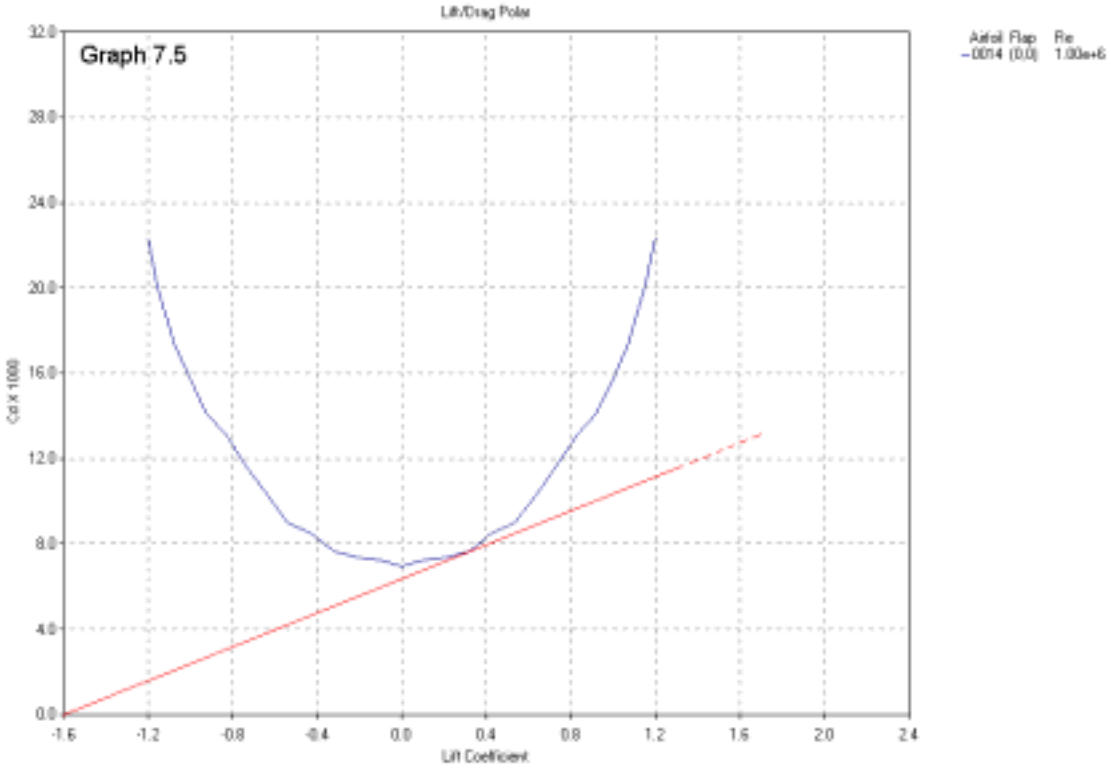

The point at which the red line makes a tangent with the blue curve therefore represents the most efficient (C_L,C_D) co-ordinate for the wing. For the chosen foil 0014, this point can be seen to correspond with and AOA ≈ 3° - see Tables 7.1 and 7.2.

Visual Foil uses the *Thin Airfoil Theory* and the *Natural / Artificial Transition Model* for CFD analysis of the chosen sections. Although the program can be used to model surface roughness on the foil, this value was left set to 0. This setting, and the values output (Graphs 7.5 and 7.6) for boundary layer thickness have implications on the manufacturing quality and surface finish of the sections.

Matching foils dimensions to force values found (Chapter 5)

Having found an appropriate foil code and operating / design AOA, *Visual Foil* was then used to ascertain the correct dimensions for the foils as specified by the calculations made in Chapter 5. Table 7.2 shows a simple iterative process used to find the foil spans required for a chosen Chord length of 0.18m. In order to enable these calculations, *Visual Foil* also requires the flying speed of the foils to be specified. The speed of the foils was set at $8ms^{-1}$ (approx. 16 knots), a speed designed to be safe, being siginificantly less than the typical water-skiing speed, and yet practical in terms of the typical operating speed of a boat and small outboard (testing considerations).

The speed does however represent that of a large ocean wave, where the speed of a wave is typically equivalent to its height in feet, i.e. a 16ft (5m) wave. By across the face of a smaller wave, a suitable speed could be generated, but the wave height does not represent the common wave height for waves found off the shores of the UK.

In order not to exceed the specified safe $8ms^{-1}$ flying speed, the nearest span dimension giving the lift force above that required was chosen. This implies that the foils should fly at a slightly slower speed than specified. This small additional force

should simultaneously account for lift loss due to wing tip vortices, although the inclusion of end plates in the design should keep this loss to a minimum.

The span dimensions chosen represent the total length of each pair of wings, B,C and D. In order to fix the wings to the main strut, half the total designed span was mounted on one side of the strut, and the other half of its length on the other side. This can be seen in the final design assembly drawing.

The simple iteration procedure gave the final design foil dimensions as follows (Force values are given to the nearest 1N):

Wing	Chord /m	Span / m	Area /m^2	AOA / degrees	Aspect ratio (Ratio Span:Chord)	Lift force / N
Wing B	0.18	0.55	0.099	3	≈ 3.1	1020
Wing C	0.18	0.24	0.043	3	≈ 1.3	445
Wing D	0.18	0.40	0.072	-3	≈ 2.2	-742

The relative proportions as described by the aspect ratio, have been kept similar to the Airchair foil. By keeping the aspect ratio fairly low, the moment (load at CP × distance to CP) applied to the mounted end of the foil is reduced, lowering the specification for the structural members carrying the wing loads. By reducing these cantilever loads, it was possible to use suitable cylindrical steel bar that fit within the section of the foil (see Chapter 8).

As mentioned in Chapter 5, incorrect sizing of the moulds meant that the sections produced had a shorter Chord than planned, being only 0.17m. After re-calculating the lift values, and loading for Wings B-D, new dimensions were found for the wings with more work in *Visual Foil*. In order to keep the new wing dimensions and specification as similar as possible, both the working AOA and wingspan were adjusted to cope with the change in specification load (700N to 800N) and chord length. By varying both values, only small changes were required:

Wing	Chord /m	Span / m	Area /m^2	AOA / degrees	Aspect ratio (Ratio Span:Chord)	Lift force / N
Wing B	0.17	0.56	0.095	3.2	≈ 3.2	1047
Wing C	0.17	0.24	0.041	3.2	≈ 1.4	449
Wing D	0.17	0.40	0.068	-3	≈ 2.4	-700

These adjusted dimensions and AOA were used in the manufacture of the prototype.

7.3 Flow considerations for the foilboard assembly

In order not to disrupt the flow over the wings to the point of significantly reducing lift, the rest of the design has been streamlined. The moulds used for Wings B,C and D were also used to make the main strut, running from the board down into the water.

The joint between the main strut and the pair of wings making up Wing C (the control wing) has been made by superimposing an extrusion of the section in perpendicular directions, so as to leave no vortex inducing edges standing proud of the section profile.

The main fuselage and clamp components on which wing pairs B and D are mounted have been machined such that the leading edge / nose of the assembly is also a NACA 0014 section. Similarly, the tail of the fuselage assembly has been boat tailed to a trailing edge design taken from Dr Li's personal studies.

At the connection between the board and main strut, the joint has been kept as simple as possible, so that the section butts up against the flat area on the base of the board. Without streamlining this area and the main strut

The drawings of the parts discussed above can be found in Appendix A.

Chapter 8 The manufacture, assembly and refinement of the design

Having generated a theoretical model for the final design based on a working assembly, and finding the desired foil sections for lift, down-force and streamlining, CAD work was used to finalise dimensions and positions of fittings. Appendix A contains detailed drawings generated for the manufacture of the device. Figure 8.1 shows the final design.

Figure 8.1 – A partially exploded view of the final design - foil assembly for the prototype

The manufacturing was shared between the Main Engineering Workshop, who produced the metal components including the load bearing members, main fuselage and clamps; the IMC who laser cut the rib master pattern profiles and the vortex control end plates: and the ATC who helped with advice and assistance on the use of composite materials.

Where possible, for the required metal components, stainless steel has been used, favouring its resistance to corrosion in salt water. Where this has not been practical due to expense and weight (see drawings for assigned materials) high grade aluminium has been chosen. With hard anodising, these components can be made salt water resistant, although this has fallen outside of the budget. For testing purposes, the useful lifespan of the aluminium will be more than sufficient.

Marine plywood has been used for the ribs (profile section bulkheads) as it is manufactured with water resistant laminating adhesives. An epoxy adhesive, *G5 Epoxy* made by *Red Head Anchoring Systems* was suggested suitable plywood to GRP and GRP to GRP bonds, by composites systems company *Scott Bader*

The glass fibre used was from *SP Systems*, a medium-weight fabric in the E-glass category, which was used in conjunction with the company recommended polyster resin *Crystic 489PA*, which was later substituted for a very similar resin *Crystic 471PALV* both made by *Scott Bader*. The switch was made after difficulties with the company-manufacturing timetable. The safety data sheets for the materials, and the corresponding catalyst hardener *Butanox M50* can be found in Appendix D. The composite is salt water resistant, UV resistant, cheap, and of average comparable strength. The composite is also suitable for hand-laying.

Comprehensive data for the mechanical properties of the composite are available at: http://www.spsystems.com/.

8.1 Using load forces found to choose structural members

For ease of manufacture and purchase, the load members chosen for incorporation in the wing sections B,C and D, and the main strut are all circular tube section stainless steel. The following hand calculations are for the members chosen for the final design.

All the load bearing members used are contained within, and attached to foil sections capable of generating lift with a non-zero AOA. For this reason all members except for those supporting wing pair Wing C are positioned so that there centre of flexure falls as close to the quarter chord position (centre of pressure) as possible. In the case of the main strut, this meant positioning two members eitherside of the quarter chord position in order to provide the necessary strength in the confined space of the profile. Wing pairs B and D are supported by members running along the quarter chord position, and have been selected to sufficiently support the bending and shear loads applied by the wings they support.

Given the comparitively small load generated by wing C, and the short span of the pair, the members have been positioned solely for practicality, irrespective of the quarter chord position.

Members contained in the main strut:

As the members contained in the main strut will be predominantly be subject to compression, resulting from the lift force from the wings, and weight of the rider, the members will be checked to see if they can cope with the buckling load applied:

Euler Buckling:

The Euler buckling load is expressed $F_E = \dfrac{EI\pi^2}{L_E{}^2}$

Due to the inertia of the board and rider relative to the foil assembly, the main strut has been modelled as a fixed / free bending condition, with the connection to the board modelled as the fixed end, and the foil assembly as the free end.

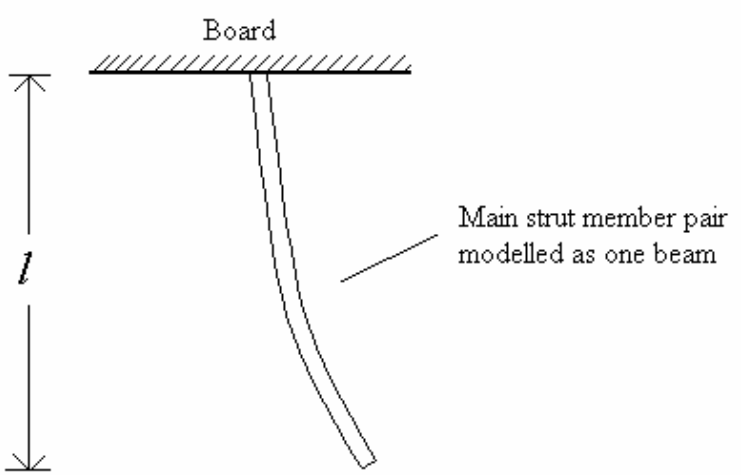

$\therefore \quad L_E = 2L$ for the main strut, L = 0.7m $\therefore \; L_E$ = 1.4m

By assigning values for E and I the buckling load F_E that the members can support can be found. I will be found first from the cross-section of the member:

The tubing chosen for the strut members is stainless steel circular section:

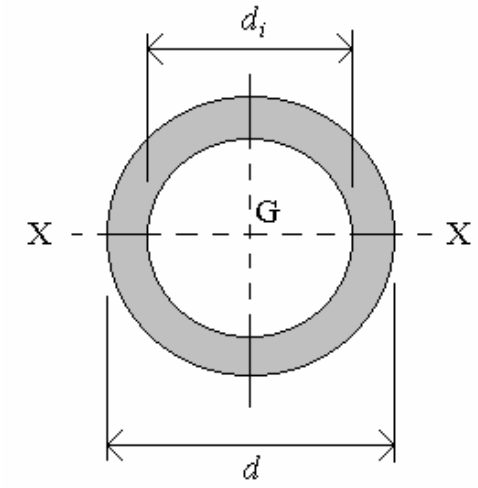

$$I_{XX} = \frac{\pi}{64}\left(d^4 - d_i{}^4\right)$$

d_i = 0.013 m (13mm)

d = 0.017 m (17mm)

$$\therefore \quad I_{XX} = \frac{\pi}{64}\left(0.017^4 - 0.013^4\right)$$

$= 2.698^{-9}$ (to 4 sig. fig)

E is taken from the value for mild steel E = 210 Gpa

Having found the variables for the Euler buckling expression, the value for F_E can be found:

$$F_E = \frac{\left(210 \times 10^9\right) \times \left(2.698 \times 10^{-9}\right) \times \pi^2}{1.4^2}$$

$F_E = 2850\ N$ (to 3 sig. fig.)

The load on the pair of members will typically be 800N. As this buckling load is only for one member, the pair together will provide a resistance to the load greater than double F_E due to the increased distance of material from the neutral axis. Much of the buckling load will also be taken in the structure of the wing surrounding the strut members, meaning that the members will safely cope with the likely buckling load by a factor of nearly 10.

Members contained in wings B and D:

The likely mode of failure of these members is through bending and shearing. Although calculations were carried out for the members, the values found suggested that the wings were over-engineered for the job, being able to support a shear load of nearly a hundred times that produced by the lift of the wings.

Shear load generated by wings = 2.49 Mpa

Shear load supported by members = 215 MPa

The decision was however made to stick with the size to keep the cost of ordering the material to a minimum. By choosing the same section as the main strut members, the order was significantly cheaper.

8.2 Manufacture and assembly procedure:

The following work was completed in the ATC Workshop, University of Warwick. The appropriate safety risk assessment can be found in Appendix E The sections below cover the work that I have personally undertaken (excluding some machinery work done by trained technicians for safety reasons). The practical experience and understanding of composite materials and design gained from the work has been an valuable part of the project.

Step 1 To secure a successful result, two copies of the mould were made, a male mould constructed of wooden ribs, 0.4mm model making maple plywood, threaded bar (studding) and nuts to secure the ribs in place. The 10mm plywood ribs were cut from a master pattern, which in turn was laser cut from the original CAD exported DXF, thus giving a very accurate profile. The ribs were initially glued to the veneer with PVA wood glue.

Step 2 After some initial test mouldings, the varnished surface of the moulds was coated with a further protective layer of chopped strand matt (random directional glass fibre) and polyester resin. In an attempt to speed the curing rate of the moulds, the composite was heated in an oven.

Step 3 The curing temperature was accidentally set too high, causing the moulds to warp. The warping caused some of the contacts between the ribs and veneer skin to break. The seems were re-glued, and the moulds straightened with ties on a secure base board. The important surfaces of the moulds remained un-harmed.

Step 4 After drawing up a plan for the manufacture of the GRP foil ‘skins’ relating to the most satisfactory areas of the two moulds, the moulds were waxed, and then, the lay-up for the first skins was made. The image here (previous page) shows three separate sections of GRP skin.

Step 5 Once dry (approx 12 hours), the skins were carefully removed from the moulds, so as not to damage the surface. The process was repeated to generate all the required half profile skins.

Step 6 A second hand surfboard was used as a base for the prototype hydrofoil. The board was cleaned, sanded, marked out and cut to take the mounting block to which the foil would attach.

Step 7 The underside of the cut hole was covered with a 2mm sheet of aluminium, slightly bigger than the hole. This plate was glassed in plate with a two layer lay-up over the plate. Once cures, the board was flipped over, and the remaining pocket filled with heavy chopped strand glass mat and resin. The large volume of resin used to make the block caused the resin to overheat on curing (a strong exothermic reaction), resulting in small bubbles forming in the composite, a possible weakness in the final piece.

Step 8 Once cured, the top-side of the mounting block was covered with a similar plate, using pre-pregnated (with resin) glass mat to compensate for the bumpy surface of the board, and a give solid level surface to aid accurate attachment of the foil assembly.

Step 9 As with the lower surface of the board, the area surrounding the aluminium plate on the top of the board, and the plate itself were covered with two layers of GRP, securing the plate in place, and acting as a method of distributing the loads anticipated from the foil assembly over the whole board.

Step 10 The plates and resin block were then drilled (8mm) and counter bored (17mm) to receive the structural members protruding from the end of the main strut.

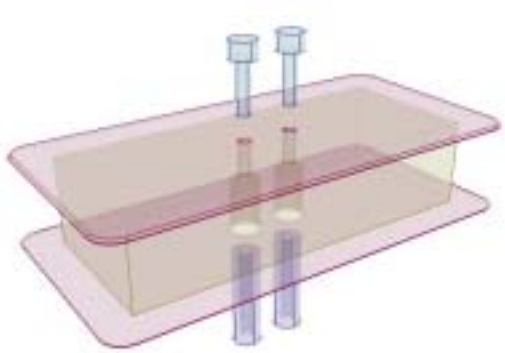

The left of the two diagrams above shows an exploded view of the resin block, plates, bars protruding from the top of the strut (shown in blue at the base of the picture) and the bolts used to hold these bars in the counter-bores.

Step 11 An aluminium block was used to mount the control wings (Wing C) on the main strut. In order to obtain a tight bond between the two parts, and maintain a clean finish at the join, the parts were combined with an

interference fit. The steel cross pieces (load members extending in to wings of Wing C) were frozen, and the main block heated. At these temperatures, the parts were then tapped together in position, and allowed to return to room temperature, leaving a tight secure bond.

Step 12 The following work was completed at my own workshop at home. The appropriate risk assessment has been included in Appendix E. Similar to the ribs produced for the moulds, a series of ribs were also cut for the wing sections, although this time, with a profile on both sides. To cope with poorly sized stock tubing for the strut and wing load members, the holes made in the ribs had to be enlarged using this home-made tool.

Step 13 Once adjusted, the ribs were measured and glued in place with two part *G5 Epoxy*. A similar process was used for wings B and D, and for the strut and wing C assembly as shown in the diagrams below.

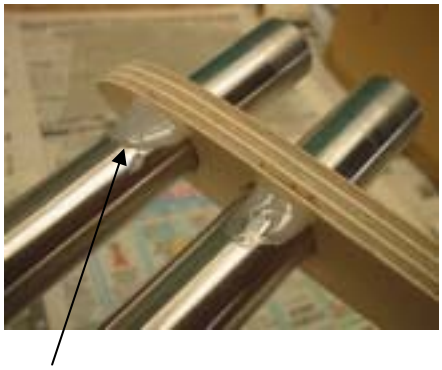

Epoxy resin fillet to secure bars to ribs during wing construction.

Step 14 The load carrying members of wings D and B were wrapped in strips of GRP, after a ‘key’ was generated on the beams with coarse sand paper. The same method was also used for the double beams of the main strut and the Wing C pair.

Step 15 One side of the profile, a ‘skin’, was then glued to one side of the rib profiles leaving the other side, and load members exposed. The *G5 Epoxy* was used as a bead along the edge of each rib to supply a strong consistent bond. Whilst curing, the skin was clamped firmly in place.

Step 16 Turning the wings over, with the ribs exposed, the load members were then secured to the CRP skin, with pre-pregnated strips of glass, a technique designed to utilise the strength of the profile skins.

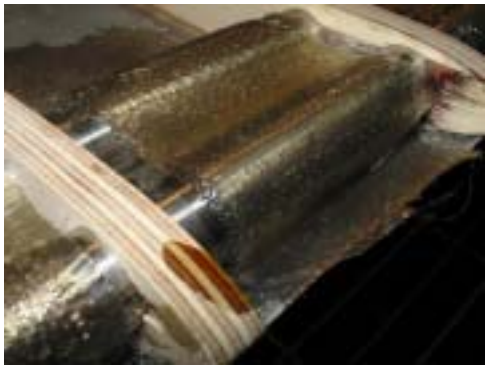

The bond was completed with a resin fillet poured and left to set along the front and back edges of these strips.

Step 17 The wings were turned over and the other skin bonded to the exposed ribs, so as to leave a gap along the leading edge, and a tight seam (with the skin below) at the trailing edge. Once the skin was set in place, strips of pre-pregnated glass were brushed into the gap between the GRP covered load member and skin, to provide a similar, but slightly inferior bond to that connecting the other skin.

Step 18 The leading edges of all the sections were created in two stages. Firstly a narrow tape of glass fabric was pre-pregnated fairly dry (minimal resin), in order that it could then be draped over the leading edge, and painted to the skins either side without sagging. Too much resin, and the unsupported fabric sags between the protruding ribs. The weaker, dry composite was then covered, once cured, with a resin rich, wider tape of glass. The GRP in this position is also expected to improve the strength of the wings by bonding the two skins. The two different widths of glass tape are expected to help spread loads from one skin into the other without leaving a week seam

Step 19 The trailing edges of all the wings were straightened and glued with *G5 Epoxy*. Strips of planed hardwood, and clamps helped to remove some of the warped features of the mould, inadvertently incorporated in the finished skins.

Step 20 To enable shaping of a sharp accurate trailing edge, two strips of glass tape were painted on either side of trailing edge of the foils, temporarily increasing the chord of the section. Difficulty was encountered trying to manufacture the seam without incorporating bubbles into the curing composite. Although they are unlikely to have much affect on strength, some difficulties were encountered when shaping the edge.

Step 21 Having generated GRP leading and trailing edges on all the sections, the profiles were then carefully sanded to give a smooth surface finish and to bring the chord length down to the required size. **It is very important to sand and cut**

GRP composites using a suitable breathing mask, and long-sleeved clothing, in a well ventilated area (see Appendix E for further details)**.**

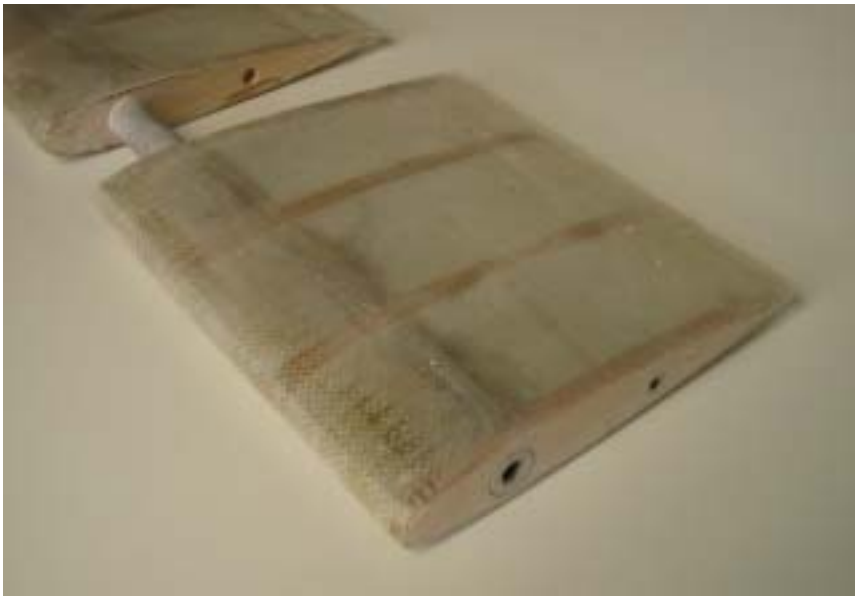

Chapter 9 Limitations of the hydrofoil

The material covered in the previous Chapters has focused on the areas where hydrofoils excel over rival displacement and planing craft, in speed, minimal drag, and ability to cope with adverse surface conditions. However, the hydrofoil inevitably has its limitations.

9.1 Control

Perhaps the largest hinderance to the growth in the use of hydrofoil based craft is the difficulty in controlling them. By taking the craft predominantly out of the water, and above the free surface, the freedom of movement in attitudes of roll, yaw and pitch are greatly accentuated over that of a displacement or planing craft. With the craft being above the free surface but close to it at all times, the boudaries for movement are very specific, and cannot be safely compromised at speed. As the benefit of the hydrofoil is to provide superior speed, this limitation is significant. If the part of the initial planing or displacement hull of the hydrofoil craft touches the free surface in flight, as a result of a freak wave, gust of wind or pilot mistake, the sudden increase in drag can impart huge impulse forces on the craft which can be detrimental to its structural intergrity, and hence the safety of the passengers. The necessary slenderness of the supporting struts makes design against this event very difficult.

Over the past hundred years a huge amount of effort has been put into the development of systems for controlling the flying height and balance of hydrofoil craft. Although many designs have been shown to work, most are only partially successful, and appear cumbersome in their solution to the problem. Ladder foil

arrangements and surface piercing foils, originally considered the solution to passive constant lift control, have commonly been criticised for their interferrence with the free surface, and the drag that this imparts on the craft. Both of these systems work by using the variation in lift with speed to adjust the amount of lifting surface submerged and in use. The hoop surface piercing foil and first ladder foil arrangement can be seen in Figures 1.2 and 1.3.

I came across a more sucessful constant lift design on a visit to engineer, and hydrofoil design pioneer Joddy Chapman's workshop, South Brent, Devon. Chapman has built to very successful hydrofoil based catamarans, the *Calliope* and *Ceres*, both sailed in the country's leading high-speed sailing innovations festival, *Speed Weeks* held in Weymouth every autumn. Both craft incorporate a trailing wand constant lift system.

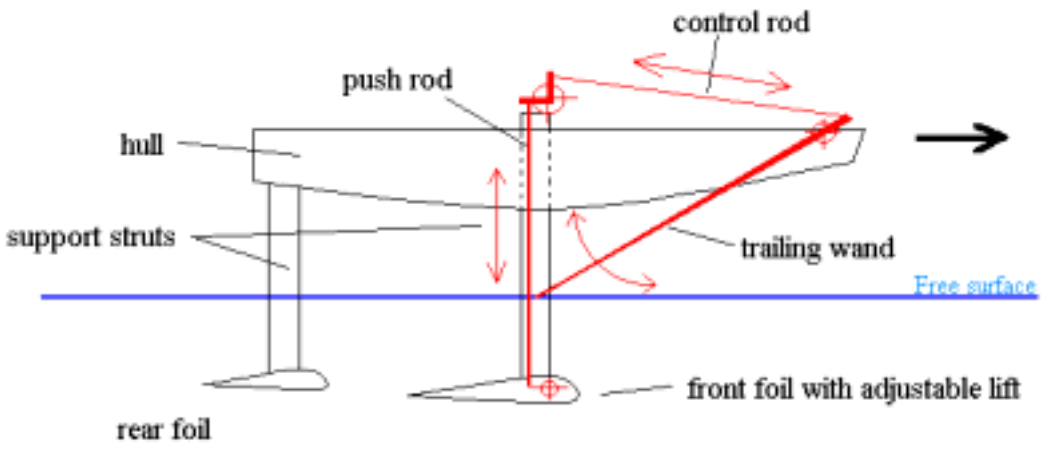

Figure 9.1 – Trailing wand method of constant lift control

The trailing wand pivoted at the end attached to the bow of the boat, planes on the free surface of the water. Its tip is positioned such that it is in line with the support strut, directly above the foil. If the speed of the craft drops, the lift generated by the foils is reduced, causing the boat to fly lower in the water. The trailing wand remains planing on the waters surface, and in the process causes it to pivot about its mounting

point. The other end of the trailing wand is attached to a control rod, which moves left to right, relative to the respective raising and lowering of the wand. A similar pivot mechansim attached to the top of the main strut is used to raise and lower a push rod built into a hollow channel in the strut section. The main foil is pivoted at the quarter chord position, and attached to the push rod at a position behind the pivot. The resulting effect is that the AOA of the foil adjusts according to the position of the push rod, which in turn adjusts according to the height of the trailing wand.

When the boat gets close too the free surface, the wand rises, pushing the trailing edge of the foil deeper, and increasing the AOA and hence generating more lift. If the boat flies too close to the free surface the reverse happens, reducing lift, and lowering the craft to the desired working depth. The mechanism is repeated on the other hull of the catamaran, attached to another lifting foil assembly. The two systems work independently of each other to provide a stable sailing platform.

Although perhaps the most successful method of control available, I believe that valuable lessons can be learned from the *Airchair* foil, and its use as the exclusive form of lift on the rider. In this instance, the rider controls the foils directly by positioning their weight, acting as the system of feeling, response, feedback and action. If this could technique could be successfully incorporated into large craft and sailed by an experienced sportsman/woman, the results would be astounding.

Another control concept of my own design, to be incoporated and studied in further work on the project would be to use self compensating foils, whereby the foil could self adjust its profile to match constant lift to variations in speed. By making the foil

from a flexible material that could deform under the varying pressure field over a wing, the amount of lift generated by the foil could be made to increase or decrease with variations in speed, keeping the craft at a constant flying height. The system would have the advantage of simplifying control to a greater degree than the trailng wand mechanism, and containing the entire system with the foil itself.

This concept of control can clearly be seen in the hovering flight of the Kestrel. In order to catch its prey, the bird will hover approximately 50ft above the ground, keeping its head incredibly still to enable it to focus on tiny ground movement. The rest of the birds body is constantly adjusting in real time to the turbulent flow rising of the coastal cliff environment in which they inhabit. The birds wings can be seen to constantly adjust to the flow, even becoming ruffled in order to dump lift during periods of fast flow – a fascinating approach to control.

9.2 Cavitation

Cavitation is not a problem exclusive to hydrofoil craft, but whereas it can be tolerated in other craft, the cavitation of the foil sections can be detrimental to the functioning of a hydrofoil boat, causing instantaneous loss of lift, sending the craft crashing into the water.

Cavitation is caused by regions of flow reaching the vapourising temperature of water, and manifesting themselves as bubbles of high temperature gas. The aerated flow over the foil causes rapid loss of lift. The problem is accentuated by the damage caused as these bubbles collapse, transmitting their high temperature to the surface on which they formed. The force and temperature of these collapsing bubbles can do

massive damage to the foils. The problem is avoided by choosing suitable section profiles so as not to generate regions of extreme low pressure. Many years of research into turbine technology has provided engineers with the tools and theory required to make a decent attempt at avoiding cavitating flow.

Chapter 10 Conclusions and indications as to the future content of the project.

10.1 Conclusion

The theory discussed in Chapters 4-6 provides conclusive theoretical evidence for the superior lift:drag ratio of hydrofoils, and the advantage that this gives a high speed water craft. For a foil and planing plate of equivalent dimensions (plan area) we can describe this superiority by assigning arbitrary, relative values to the two mechanisms:

Ratio lift:drag	Planing plate	-	4:2
	Hydrofoil	-	8:1

However due to complexity of variables involved in such a fluid problem, the theory must be grounded in practical work to validate this conclusion. Due to timing difficulties with a single component commissioned to the Engineering Main Lab for manufacture, it has not been possible to provide a photo of the finished piece, although it will be available for the project oral presentation. As the prototype has only just been completed, it has not been possible to provide test data as planned in the progress report.

As the project has been put forward and is likely to be used as a fourth year project for 2003 / 2004, testing work will be carried out over the summer period, in order to provide a sound base on which to build an improved prototype.

Although not yet under test, the finished prototype confirms the success of the design and manufacture work completed, producing a very strong composite structure, to the

load specifications set in Chapter five. Although the design is not as lightweight as it might be, I believe it is likely to compare favourably with the commercial *Airchair* foil, made from solid aluminium. A degree of design excess in the load members chosen indicates a focus on this area of design for the next prototype. This excess of strength in the design will however, provide a safe platform for testing.

10.2 Further work, and related topics and areas where technology might be applied.

As mentioned above, the project is in the process of be submitted to the fourth project list in time for 2003 / 2004. I believe that the work completed in the project so far and testing to be completed over the summer provides a sound basis for further work on the topic for both third and fourth year students.

The breadth of the subject and the material I have covered in the report only touch the surface of the work and progress that could be gained from further study. I have found the material involved very useful and interesting, covering a wide variety of engineering design and theoretical principles.

All the prototype made has been designed as part of a surfboard, I feel the project has more direction, and direct application in the sport of sailing, where more money and enthusiasm towards product development can be found. The lessons learned from the *Airchair* solution to creating a stable flying platform with only one foil could be directly applied to a racing dinghy, perhaps providing a successful rival to the popular *Windrider RAVE*.

As well as furthering the sophistication of the prototype design, significant work should be invested in development of testing apparatus for the foil, as it is difficult to provide valid CFD data and / or wind / water tunnel work to support the theory discussed. This work will involve the use of strain gauges and flow-speed measuring devices that can be used in conjunction with a data logging unit.

I would also like to see further work and the development of theory surrounding the use of self-adjusting, flexible foils, as briefly discussed in Chapter 9.

Bibliography

- Prandtl and Tietjens,
  Applied Hydro- and Aeromechanics,
  Edition (unknown), Dover Publishing, original publication, 1934,
  Pgs – 144-225.

- Saunders, H. E.,
  Hydrodynamics in Ship Design, Volume 1,
  1st Edition, Published by the Society of Naval Architects and Marine Engineers, 1957
  Extensive material used.

- Saunders, H. E.,
  Hydrodynamics in Ship Design, Volume 2,
  1st Edition, Published by the Society of Naval Architects and Marine Engineers, 1957
  Extensive material used.

- Коуин, H. E, et al,
  Theoretical fluid mechanics,
  Published – Moscow 1952
  Pgs – 336-343

- Sedov, L. I,
  Two-dimensional Problems in Hydrodynamics and Aerodynamics,
  Interscience Publishers, 1965
  Pgs – 239-281

- Gordon, J. E,
  Structures *Or Why Things Don't Fall Down*,
  5th Edition, Penguin Publishing, 1984
  Pgs – 259-271

- Shapiro, A. H,
  Shape and Flow *The fluid dynamics of drag*
  4th Edition, Heinemann Publishing,1977
  Extensively read for background understanding and confirmation of drag on foils.

Text References

[1] Hayward, Leslie, "**The History of Hydrofoils**," *Hovering Craft and Hydrofoils*, Vol 4. No. 8 (May 1965) through Vol. 6, No. 6 (Feb 1967).
– as referred to by http://www.foils.org/gallery/early.htm - the site from which the material was taken.

[2] Dixon, Malin, http://www.foils.org/gallery/forlani.htm, **Forlani**, -visited Feb 2003.

[3] Marcus, Ben, http://www.surfingforlife.com/, **The History of Surfing From Captain Cook to the Present**, - website containing a detailed account of the history of Hawaiian surfing.

[4] A comprehensive explanation of the evolution of the theory can be found in: Prandtl and Tietjens, **Applied Hydro and Aeromechanics**, (see bibliography), pgs 173-184.

[5] Li, S. C, **Turbo-Machinery,** University of Warwick, Lecture series, pg 3-21

[6] An in-depth derivation of the formulae used can be found in: Коуин H. E. et al, **Theoretical Fluid Mechanics**, (see bibliography), pgs 337-343.

[7] Again, a comprehensive explanation of the material can be found in: Prandtl and Tietjens, **Applied Hydro and Aeromechanics**, (see bibliography), pgs 198-225.

[8] Gordon, J. E, **Structures** *Or Why Things Don't Fall Down*, Edition 5, Penguin Books Publishing, 1984, pgs 259-271.

[9] Further work on a more sophisticated model can be found in: Paine, Michael, **The Hydrodynamics of surfboards,** 1974, Sydney University.

Image References

[i1] Dixon, Malin, http://www.foils.org/gallery/forlani.htm, **Forlani**, - visited Feb 2003.

[i2] Meyer, John, **"Ships That Fly",** - as referred to by - Dixon, Malin, http://www.foils.org/gallery/forlani.htm - visited Feb 2003.

[i3] (no author available) - http://www.foils.org/gallery/phm.htm - visited Apr 2003.

[i4] Marcus, Ben, http://www.surfingforlife.com/, **The History of Surfing From Captain Cook to the Present**, - website containing a detailed account of the history of Hawaiian surfing. Website visited Apr 2003.

[i5] (no author available) - http://www.windrider.com/wrrave.shtml, - **The Windrider Rave – an innovative hydrofoil trimaran –** website visited Jan 2003.

[i6] Osgood, Bambi - http://www.airchair.com, - website visited Oct 2002.

[i7] -as [i6].

[i8] Manny, Mango - http://www.hydrofoilsurfing.com, **Hydrofoil Surfing Headquarters**- website visited regularly between Sept 2002 and Apr 2003.

[i9] -as [i8].

[i10] -as [i8].

[i11] **Surfers Path Magazine**, Dec 2002